3
Sweet-spot estimation of depth to the top of magnetisation

C.A. Foss

ABSTRACT

It is commonly assumed that any segment of magnetic field data can automatically be inverted to create a space-filling model of subsurface magnetisation. This is true, but unless the magnetic field data carries information required to reasonably constrain magnetisation models there will be no value to any models generated from it. Any degree of confidence in even the most reliable space-filling models applies only to a small proportion of the model volume. I refer to the locations where the magnetic field carries significant source information, the measurements at those locations and the subsurface magnetisation contrasts giving rise to those field variations collectively as 'sweet-spots'. Because of non-uniqueness, no magnetic field data is truly diagnostic of its source magnetisation. However, suitable segments of data provide reliable source models with only simple and generally reasonable assumptions. Away from these favourable data segments, confidence in recovered models falls abruptly giving an almost binary classification of sweet-spots where information can be reliably recovered and 'other' areas where the magnetic field is only weakly informative about subsurface magnetisation. A necessary condition of a sweet-spot is that the magnetic field contains a discrete feature for which the curvature can be ascribed to a single discrete magnetisation. These are generally the shallower magnetisations in an area.

Depth to the top of a magnetisation is a detail of its distribution and can only be recovered for stated model assumptions, generally that the magnetisation has a horizontal top and sharp edges. As an alternative to specific source geometry, structural indices can also be used to summarise the distribution of a magnetisation. I provide an analysis of the sensitivity with which we can hope to recover estimates of depth to magnetisation from magnetic field inversion and illustrate this with a case study from the Sedan area of South Australia.

3.1 INTRODUCTION

A common reason to conduct a magnetic field survey is to map depth to the top of magnetisation. There is a comprehensive literature of methods to do this (e.g. Werner 1953; McGrath and Hood 1970; Naudy 1971; Nabighian 1972; Thompson 1982; Ku and Sharp 1983; Reid *et al.* 1990; Almond and Fitzgerald 1998; Silva and Barbosa 2003; Vallée *et al.* 2004; Hansen 2005). Different methods use derivations based on potential field theory and all methods necessarily include some characterisation of the the distribution of magnetisation (either as a specific shape or as a structural index). Some analyses include their own estimation of source shape from second or higher order derivatives of the field, but as outlined by Reid (1980) use of derivatives places greater

requirement on the sampling and precision with which the field is measured. In practice, measurement imperfections restrict analysis of higher-order derivatives from magnetic field measurements.

Potential field theory allows that on any surface a film of virtual magnetisation can replicate any magnetisations beneath that surface as the source of a magnetic field measured at any elevation above it (even though this requires infinitesimally detailed variation of unacceptably extreme magnetisation intensities). As impractical as this solution may be, it highlights the challenge of establishing a minimum depth-to-magnetisation. It is commonly assumed that depth to its top is one of the most pronounced and easily recovered statistics of a distribution of magnetisation, but for compact sources this is not true. Figure 3.1 shows a magnetic profile over concentric sources with top depths of between 20 and 250 m below the measurement surface. For concentric spherical sources of equal total magnetisation the magnetic anomalies are identical and there is no sensitivity to depth to the top (other than that it is shallower than depth to the centre). The co-centred cube with side length 100 m and depth to the top 250 m has an anomaly with only minor difference to those of the spherical sources, and the cubes with side length 200 and 300 m (depths to top 200 and 150 m respectively) also have quite similar anomalies.

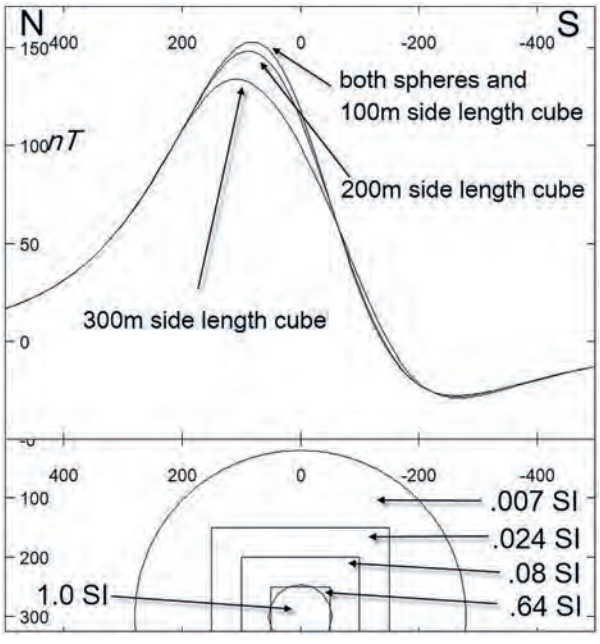

Fig. 3.1. Central north–south sections over concentric spheres and cubes of equal total magnetisation.

As shown in Fig. 3.2, differences between the magnetic fields of these sources are also difficult to discern in map view, even over the centres of the anomalies where those differences are largest. Interpretation of the significance of subtle differences between model-computed and measured fields requires close-spaced, high-resolution measurements. For the anomalies shown in Figs 3.1 and 3.2 with an amplitude range almost 200 nT the maximum differences between the fields are 15 nT for the 300 m side-length cube and other bodies, and only 5 nT between those other bodies. Figure 3.3 shows near-identical north–south magnetic field profiles over the centre of a cube of side length 200 m and depth to top 200 m and two bodies of polygonal section, homogeneous magnetisation and identical strike length and azimuth. The shallowest of the bodies has a depth to top only 50% of the cube. Equalities are not limited to such '2.5d' bodies (bodies with constant cross-section along their strike axis) but exist for any magnetised body. For inversion of measured magnetic field data, causative geological bodies are not known to be of simple geometry. However, if an anomaly can be reasonably matched using a model of simple geometry then introduction of any additional complexity must be justified. If the magnetic profile shown in Fig. 3.3 is inverted on the assumption that the source is a simple sharp-edged, horizontal-top body it should return a depth estimate close to 200 m, although either of the

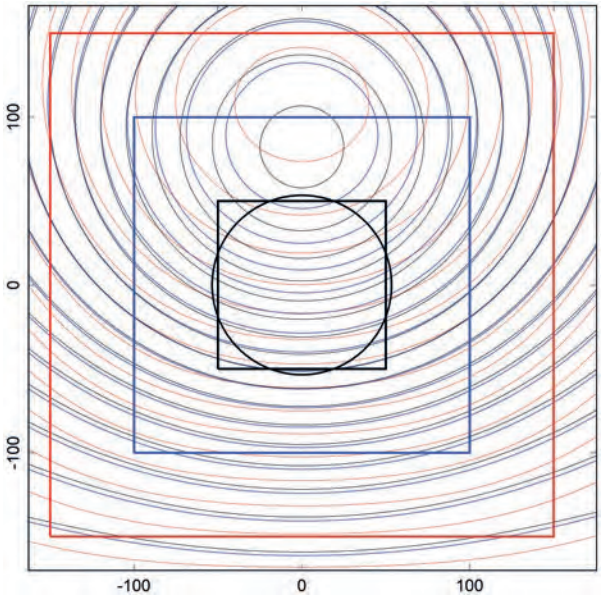

Fig. 3.2. Contour displays of the magnetic anomalies shown in Fig. 3.1. Red – 300 m side-length cube and contours. Blue – 200 m side-length cube and contours. Black – spheres, 100 m cube and their field contours. All contour intervals are 10 nT.

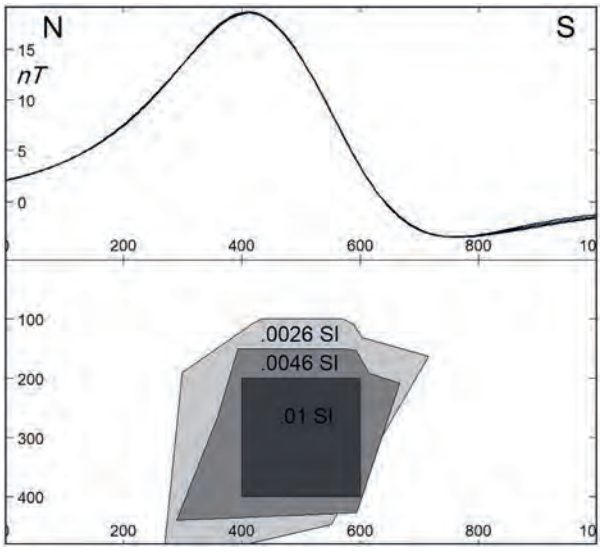

Fig. 3.3. Bodies with near-identical magnetic fields but quite different depths to top.

two shallower alternative models might represent the true magnetisation. Examples such as this reinforce the known requirement that a specified geometry is necessary rather than optional for source depth estimation. Assumption of shape is particularly important for the top surface of a model. If the assumption of a horizontal top surface is relaxed then estimation of depth to the top of magnetisation is unsupported. Fortunately, specification of a horizontal top surface is in many geological cases a reasonable assumption. For instance, in Australia many magnetic field features are due to magnetisations terminated beneath a sub-horizontal basement unconformity that is broadly consistent with this model assumption.

The most relevant statistic for evaluation of magnetic depth estimation methods is their predictive success, but unfortunately there is no definitive database recording this statistic, and almost all claims of precision in estimating depth to magnetisation have been made using synthetic data or already-known drilling results. If exploration geophysics had a regulatory authority then such a database could be created and maintained from pre-drilling predictions using block-chain authentication. Authenticated empirical results are particularly important because non-uniqueness precludes a strictly analytic evaluation of different methods and obscures the issues considerably. In this chapter I outline the method of 'sweet-spot' magnetic depth estimation. This method is subject to the same non-uniqueness limitations as for all other methods but it has a key advantage that solutions are directly tested against the field variations they are proposed to explain. Although I specifically present the sweet-spot method, the issues I discuss in this chapter apply to all depth estimation methodologies.

Sweet-spot depth estimation combines three concepts from which different implementations can be developed. These concepts are:

1) Source magnetisation information is only selectively available from magnetic field data at locations of suitable subsurface magnetisation contrasts. If the magnetic field measurements above these locations are of high quality, the location and magnetic field data define as a sweet-spot.
2) The small data package defining a sweet-spot is optimum for intensive, focussed and individually tuned analyses or inversions.
3) Magnetic depth estimates do not have conventional uncertainty statistics but can be characterised by model sensitivities with an accompanying caveat that model assumptions are valid.

Magnetic field surveys typically provide uniform data coverage. Geology, however, is not uniform. The location and characteristics of abrupt and substantial contrasts in subsurface magnetisation control the overlying magnetic field variations and determine the feasibility of recovering information from analysis of magnetic field data. Any magnetic source depth estimator should be able to return reasonable results where magnetisation distributions are supportive. If the geological distribution of magnetisation is not supportive then no method will provide reliable results.

An ideal sweet-spot is a simple magnetic field variation with amplitude well above measurement noise and superimposed field variations. The measurements should extend across several flightlines and be well separated from field variations due to other magnetisations. In Chapter 2 (section 2.8) I presented a study of sweet-spots over the Gairdner dykes of South Australia that are particularly well suited to source depth estimation. Other field variations may be less appropriate because they are too complex, overlap, or are defined by insufficient measurements. In other areas there may be no sweet-spots at all. In consequence, many depth estimation studies are a compromise between restricting the number of solutions to retain reliability of results and expanding the number of solutions to provide more information, albeit at lower reliability.

The initial recognition of a sweet-spot is as a discrete and well-sampled magnetic field anomaly. As the different

models in Fig. 3.3 illustrate, even an apparently suitable field variation can return misleading depth estimation results. However, this can only be known from subsequent testing with independent information. In consequence I classify all field variations apparently supportive of depth estimation as sweet-spots and allow that results may include some solutions seemingly well justified by the available data but which may later be shown to be misleading of the true magnetisation distribution.

3.1.1 Sweet-spot data packages

The three models shown in Fig. 3.3 produce similar but not identical fields (difference between the fields can be further reduced to any degree by adding more model complexity). To discriminate between source models from analysis of their magnetic fields requires confidence in minor features of the data. To focus on such small field differences, inversions should be optimised. Ongoing advances in computing speed and memory size permit generation of extremely large models from inversion of extremely large datasets. Small increments of magnetisation in these models contribute meaningfully to only small sections of the measured field and no part of the resulting model is optimised as well as can be achieved by isolation of smaller, local models with smaller, local data packages. Where possible, magnetic source depth estimations should ensure that results are compatible with surrounding data and models. Small models and datasets also encourage application of sensitivity tests by scanning ranges of model parameter values to investigate rates of divergence of data-fit away from the optimum solution.

After the extent of a dataset for inversion is specified, the next step is to split that data into anomalous (residual) and background (regional) parts. This operation is interpretive and generally requires inclusion of data at or beyond the margin of the anomaly. However, the data used in an inversion should not extend far beyond the anomaly as that dilutes focus on the critical data. Unfortunately, the only section of the background field that requires definition is the part overlapped by the anomaly itself, where it cannot be directly measured or easily estimated. Widening the area across which the background field is estimated does not in all cases improve fidelity of anomaly separation.

It is essential to establish the authenticity and suitability of any data to be used for magnetic source depth estimation. For methods using gridded data this includes the fidelity with which the grid represents the magnetic field. This chapter includes evaluation of source depth estimates derived from gridded data.

3.1.2 Forward modelling tests of depth estimates

Inability to prove correctness of magnetic source depth solutions due to non-uniqueness can discourage what should be best efforts to optimise depth estimation results. All depth estimate solutions should be tested by forward modelling to establish that they explain the field variation from which they are derived. This does not establish that they are correct but can readily detect solutions that are obviously inappropriate. Automation of magnetic source depth estimation generally involves tuning to generate either a small number of solutions at high discrimination, or many solutions at low discrimination. Depth estimation methods that are unable to directly interrogate solutions with forward modelling apply two styles of confidence or quality tests: (i) solutions are plotted over magnetic field images and those associated with the most distinct features in the magnetic field are attributed higher reliability, or (ii) clusters of adjacent solutions with similar value are accepted to be of higher reliability. Neither of these evaluations is a direct test of the validity of solutions other than allowing rejection of inconsistent results.

3.2 KEY PRACTICAL CHALLENGES OF MAGNETIC SOURCE DEPTH ESTIMATION

Major and overlapping sources of error in a model to explain a measured magnetic field are:

1) fundamental non-uniqueness and model insensitivity
2) imperfection or insufficiency of the magnetic field, elevation or topography data
3) incorrect separation of the magnetic field due to the magnetisation
4) inappropriate model specification
5) incorrect geological attribution of the magnetisation.

I illustrate some of these issues with synthetic data and in a case study over the Sedan area of South Australia.

3.2.1 Fundamental insensitivity of magnetic field inversion

In favourable cases of suitable geology and high-quality magnetic field data, the fundamental limitations of non-uniqueness account for a substantial part of the

uncertainty in magnetic field source depth estimates as I will show in the following investigations. In Figs 3.1 to 3.3 I illustrated how different source magnetisations can generate similar magnetic fields. I now quantify those differences and relate statistics of difference between two magnetic fields to variations in depth to the top of their source magnetisations. Figure 3.4 shows the central north–south magnetic field profiles over regular circular section cylinders, and equal volume, thickness and depth extent rectangular prisms in a field of strength 50,000 nT, declination 0° and inclination −60°. Depths to the tops of the magnetisations are 320, 400 and 480 m (400 m +/− 20%). For each source depth the magnetic field profiles of the cylinders and prisms are almost identical. For the shallower bodies there is a slight increase in amplitude for the rectangular prisms but this can be readily modified by minor adjustment of thickness, strike extent or magnetic susceptibility. The decrease and increase in depth by 20% of the central depth of 400 m causes an increase and decrease in peak

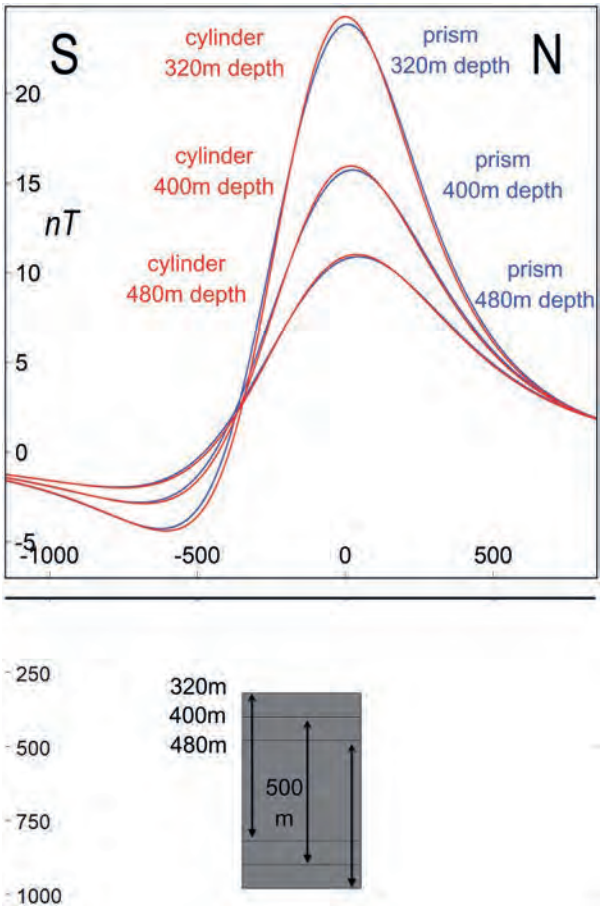

Fig. 3.4. Central magnetic field profiles over 400 m wide dodecagonal cylinders (red) and rectangular prisms (blue) at depths of 320, 400 and 480 m.

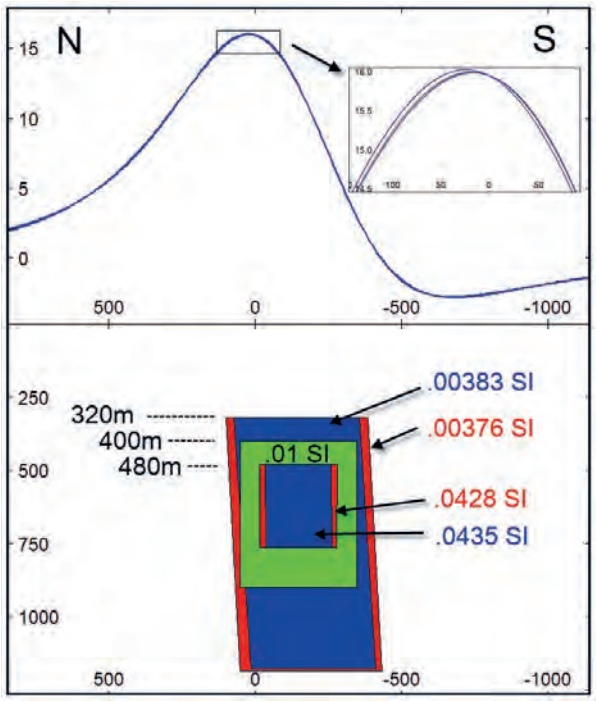

Fig. 3.5. Magnetic profiles over depth-offset prisms (blue) and cylinders (red) to best fit the profile of a cylindrical magnetisation (green) at the reference depth. The inset shows magnification of the almost imperceptible differences at the anomaly peaks.

amplitude for the anomalies of either body by +52% and −31% respectively. This compares to differences of only 1% to 2% between peak amplitudes of the two body-type anomalies at each depth. From the magnetic field profiles of Fig. 3.4 there appears to be high sensitivity to source depth for both model geometries. Unfortunately, that sensitivity is significantly reduced by compensating variation of any unknown parameters, particularly magnetic susceptibility, thickness and depth extent. This is illustrated in Fig. 3.5, in which the magnetic fields of the bodies at 320 and 480 m depth are best-fitted to the field of the cylindrical body at 400 m by variation of those other parameters. The reduced differences between field curves from Fig. 3.4 to Fig. 3.5 clearly establishes that uncertainty of the values of other parameters is the primary cause of low sensitivity to source depth. Further reduction of differences between fields from magnetisations at different depths (further increase in the scope of non-uniqueness) is possible if the specification of body geometry is relaxed.

The difference between two magnetic fields can be quantified by their percentage root-mean-square (rms) misfit. This is the standard deviation of difference between the fields normalised to the standard deviation

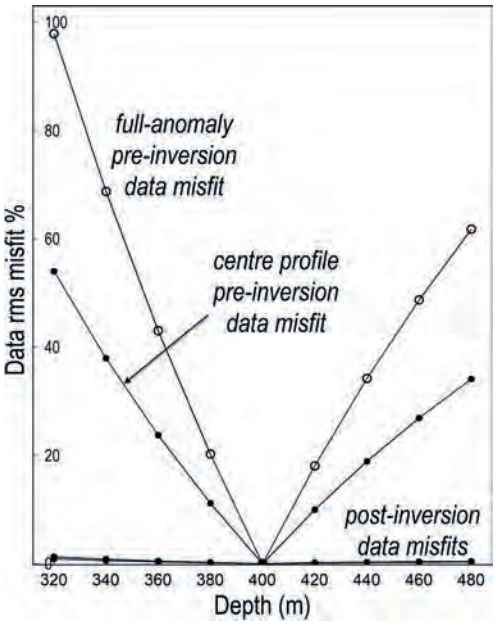

Fig. 3.6. Pre- and post-inversion misfit rms statistics for the full anomaly and centre profile of a circular cylinder at 400 m depth and best-fit cylinders at depth offsets of up to +/– 20%.

of the reference field and multiplied by 100. The statistic is directly related to objective terms minimised in inversion algorithms, including that of the Levenburg–Marquadt ridge-regression method (Marquardt 1970) implementation in the ModelVision software used in this book (Pratt *et al*. 2020). Unfortunately, it is not possible to assign an interpretational threshold to this or any equivalent statistic because their significance is subjective. The pre- and post-inversion rms misfit values both between the central profiles plotted in Figs 3.4 and 3.5 (for a single profile inversion) and between the complete anomalies (for full anomaly inversions) are plotted in Fig. 3.6. The increase by a factor of less than 2 from single-profile to complete-anomaly misfit values is of little significance because it is overwhelmed by differences in anomaly separation and weighting of model parameters between the two inversions. The similar pattern of these curves, and particularly their identical minima, supports application of central-profile analysis in source depth estimation. The key feature of Fig. 3.6 (the most informative figure in this chapter) is the 99% loss of sensitivity to source depth between the pre-inversion and post-inversion misfit values arising from uncertainty in other source parameter values. Parametric inversion is ideal to investigate these relationships but the findings are equally relevant to all other inversion methods, even if the output of those inversions are not expressed in terms of individual source parameters.

The role of individual parameters in compensating for error in estimation of depth-to-magnetisation is highlighted in Fig. 3.7. This figure plots parameter values for each of the best-fit models found by inversion at different offset depths. Figure 3.7A plots the magnetic susceptibility values. Unknown or incorrect magnetic susceptibility is a major contribution to uncertainty in source depth estimation. Increase in estimated source depth is facilitated by higher magnetic susceptibility values, and conversely decrease in estimated source depth is facilitated by lower estimated magnetic susceptibility values. Figure 3.7A plots the fivefold increase and decrease respectively in apparent magnetic susceptibility values associated with a 20% increase and decrease in estimated depth. With this ratio, the challenge of estimating subsurface magnetic susceptibility values is clearly more substantial than the challenge in estimating depth to the top of that magnetisation. There would be major advantage in constraining magnetic source depth estimates with true magnetic susceptibility values, but because of geological variability across many scales this is rarely feasible to better than an order of magnitude, even where some susceptibility measurements are available. The analysis presented here finds the single apparent magnetic susceptibility values of the best-fit models at each depth offset. Most of the variation in depth to the top of magnetisation related to incorrect magnetic susceptibility values arises from magnetic susceptibility variations within a factor of up to 3 or 4. Larger departures of the magnetic susceptibility values accommodate only slight additional depth changes.

Figure 3.7B plots the thickness of the best-fit models for each depth offset. Variation in source thickness is less substantial than the associated variation in magnetic susceptibility, with a proportional variation in thickness of approximately two to three times the proportional variation in depth. Deeper bodies have reduced thickness to compensate for the reduced anomaly sharpness arising from the increased source depth.

Depth extent plotted in Fig. 3.7C also shows an inverse relationship with depth, in this case with a scaling factor of three to four times the change in depth. The change in depth extent compensates for change in sharpness of anomalies by adding or removing long wavelength field variations from the base of the model to contribute towards adjustment for changes in depth to its top.

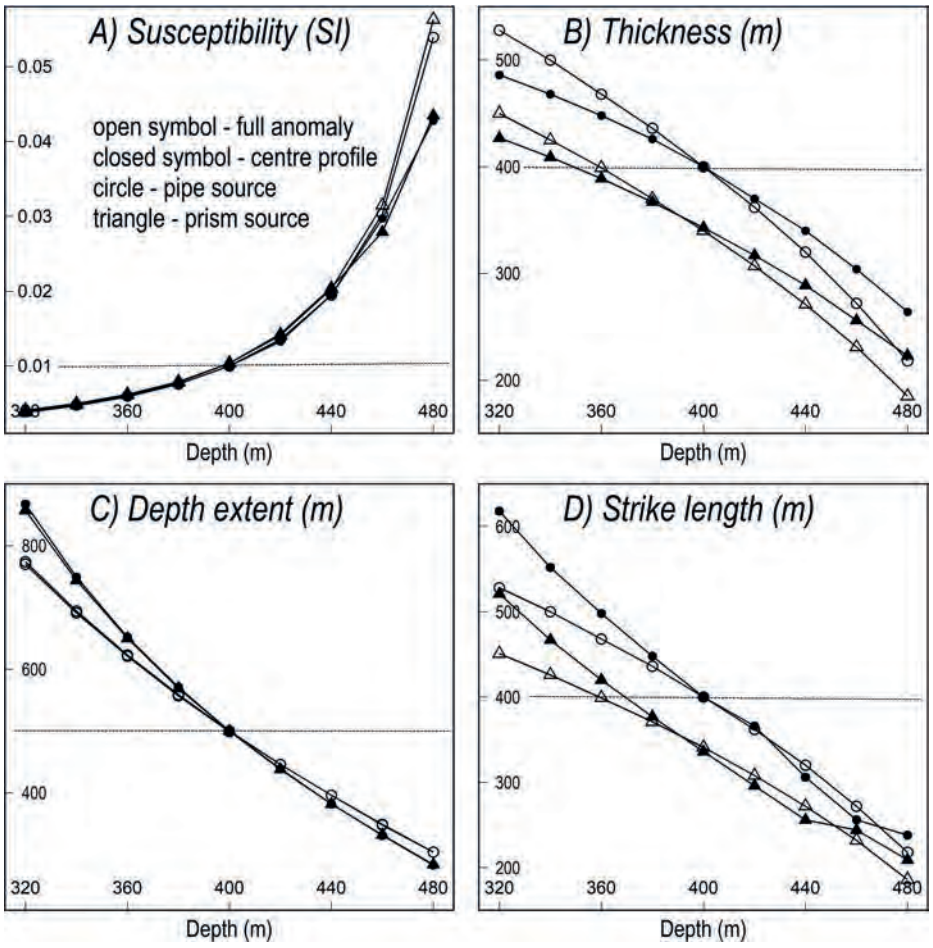

Fig. 3.7. Mapping of parameter values for the best-fit inversions at different depth offsets. Open symbols are for full anomaly inversions and closed symbols for centre profile inversions. Circle symbols are for cylinder models and triangles for prism models.

Figure 3.7D shows a near-linear inverse variation in strike length by a factor of 2 for the 20% increase and decrease in apparent depth. There is an offset between plots for the rectangular and elliptic section bodies, with larger strike lengths of the elliptic section bodies compensating for taper in width along their strike axes. The strike length of a magnetic body is almost unconstrained by inversion of data on only the central profile of an anomaly, but assigning a strike length (together with azimuth of strike) to the magnetisation based on inspection of the field variation in map view is generally sufficient to specify this parameter.

Variation in shape between the bodies used in this study is of low significance. The curves plotted in Fig. 3.7 are for both cylindrical and rectangular prism models. The parallel behaviour of each individual parameter for these two bodies supports substitution of either body type for the other in inversions to estimate depth to the top of magnetisation. The similar values and patterns of variation of the post-inversion difference statistics plotted in Fig. 3.8 (which is a vertical magnification of the post-inversion curves plotted in Fig. 3.6) also support this conclusion, with no significant offset in best-estimated depth between the two model types.

3.2.2 Data selection – single profile analysis

In the previous section I have shown that horizontal-top models of simple cross-section can be interchanged in estimation of source depth. Simple cross-section shape and homogeneous magnetisation are in most cases justified, with the exception of magnetisations at shallow depth for which there may be substantial expression of any shallow inhomogeneities. In this section I investigate analysis of individual profiles rather than complete

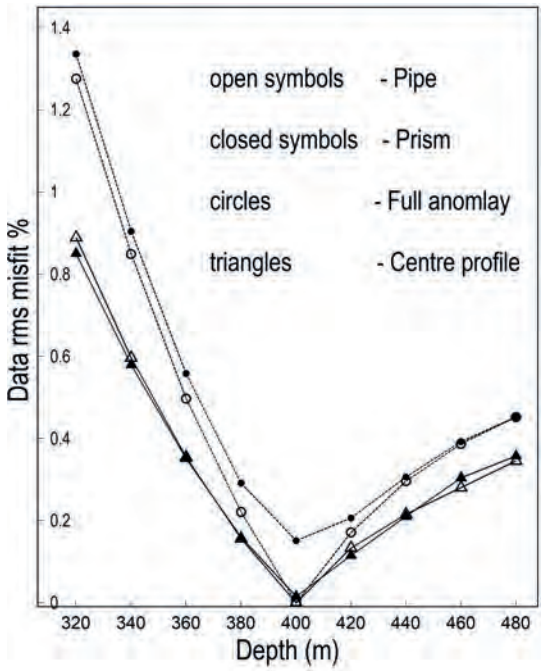

Fig. 3.8. Minimum (post-inversion) data misfit at each depth offset for full anomaly and central profile analyses of cylinder and prism models (expansion of the post-inversion curves in Fig. 3.6).

anomalies. Analysis and interpretation of measured anomalies face problems in separation of overlapping fields, particularly towards their margins. A central profile generally provides more reliable data and in some cases may be the only feasible option if other parts of the anomaly are inaccessible or are overprinted with fields of adjacent magnetisations.

Matching of a complete anomaly can provide the best-qualified bulk estimates of the magnetisation, such as total magnetisation, average magnetic susceptibility or total magnetisation and volume. Depth to its top is, however, a detail of a magnetisation, and its estimation is optimised differently. The most informative aspect of the magnetic field regarding depth to top of magnetisation is field curvature. Matching a well-positioned profile rather than the complete anomaly allows the most critical region of field curvature to be better honoured. Matching a single profile does, however, raise the additional challenge of estimating strike length and azimuth. For highly elongate anomalies, such as those due to dykes, this is not a problem as strike azimuth is well estimated from multiple profile intersections and there is little sensitivity to variation of large strike extent. For more equidimensional magnetisations, the almost linear inverse relationship between strike length and estimated depth to the top of magnetisation plotted in Fig. 3.7D reveals that an overestimation of strike length produces a tendency towards underestimation of depth and conversely, underestimation of strike length encourages overestimation of depth.

For inversion of measured field anomalies a suitable approach to address strike length is to set strike length and azimuth from inspection of the magnetic field variation in map view and to leave them fixed in the initial inversion stages. Once inversion has reduced the major data misfit, in subsequent inversion runs strike length can optionally be enabled as a free parameter. Figure 3.9 plots post-inversion data misfits for multiple cylindrical-section and rectangular-section models with fixed but incorrect strike length. These inversions allow variation of magnetic susceptibility, thickness, depth extent and dip in attempts to compensate for the incorrect strike length. For both body types, the global data misfit minima are at the true depth of 400 m. Consistent with results plotted in Fig. 3.7D, the minima of curves for bodies of erroneously large strike length provide underestimates of depth-to-magnetisation, and for bodies of erroneously short strike length the minima provide overestimates of depth-to-magnetisation. For body types of both cross-section geometries, a misrepresentation of strike length by 25% (+/− 100 m for the models shown) is

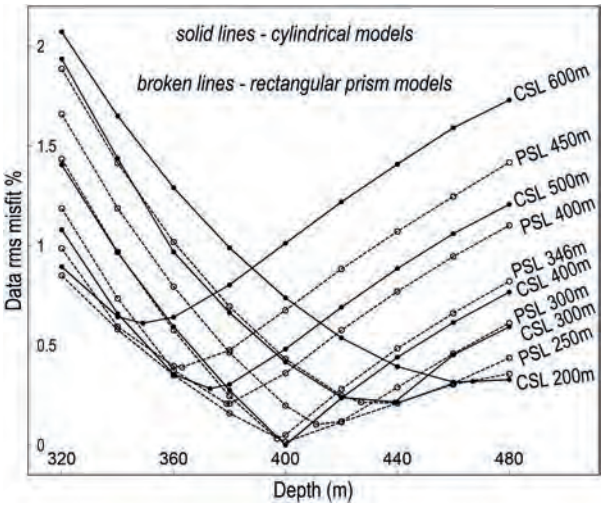

Fig. 3.9. Post-inversion data misfit curves for models of different strike length (CSL – cylinder strike length and PSL – prism strike length). The global minimum misfit at the true 400 m depth is given by the 400 m strike length cylinder and 346 m strike length prism models.

associated with an error of less than 10% in the estimated depth to the top of magnetisation.

Single profile analysis is a powerful (but not essential) aspect of sweet-spot depth estimation. The major remaining issue impacting on estimation of depth to the top of magnetisation is data sampling that I investigate in the following study.

3.3 A SYNTHETIC-DATA STUDY OF DEPTH TO MAGNETISATION ESTIMATION

Having established the fundamental limitations in estimating depth to the top of magnetisations we can now evaluate the additional uncertainty arising from overlapping fields and incomplete data sampling. For aeromagnetic surveys conducted on flightlines, inadequacy in sampling the field generally involves flightline spacing. For helicopters and fixed-wing aircraft with measurements made at 10 or 20 Hz, the along-profile spacing is typically between 1 and 10 m whereas survey line spacings are typically in the range of 20 to 400 m. In many cases this gives between-line to within-line measurement spacing ratios greater than 10. To investigate the effect of line spacing I again first use synthetic, noise-free data.

Figure 3.10 shows north–south synthetic flightlines at 50 and 400 m spacing over a set of 31 synthetic models with horizontal top surfaces, vertical plunge and different size, shape and orientation. The bodies have a range of susceptibilities from 0.05 SI for the smaller bodies to 0.003 SI for the larger bodies so that a range of body sizes contribute significantly to the magnetic field. The tops of the bodies are all at a common elevation and there is no superimposed background field. Nevertheless, even this ideal model presents considerable challenges in solution of the inverse problem to estimate depth to those magnetisations from fields at moderate elevations above them or with insufficient sampling. The field is computed for induced magnetisation in a geomagnetic inclination -60° and declination 0°. In this steep but non-vertical field each body produces a dipole anomaly with a dominant peak slightly to the north of the centre of magnetisation and a weaker negative further to the south. The magnetic field can be simplified by application of a reduced to pole (RTP) transform, but this introduces artefacts for insufficiently sampled data as well as dependence on magnetisation direction. I use TMI computed from the model in Fig. 3.10 to illustrate limitations in mapping depth to the top of magnetisation according to elevation of the measurement surface above the magnetisations, and analysis of multiple and single flightlines and grid traverses.

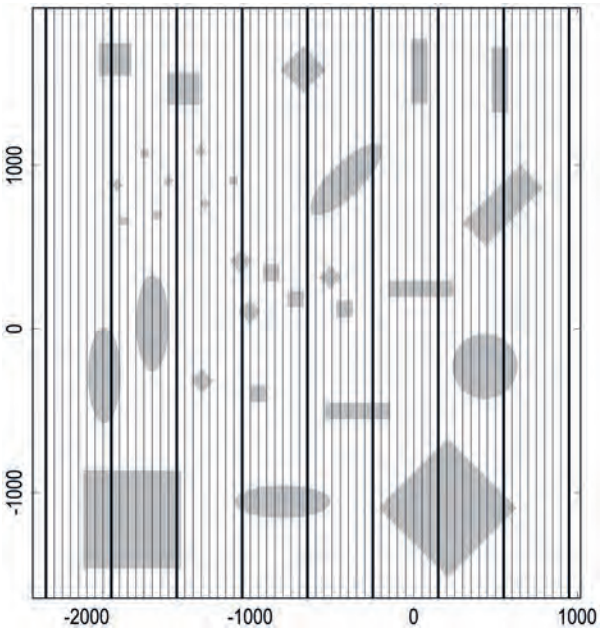

Fig. 3.10. Plan view of a magnetisation model with synthetic flightlines at 50 m (feint) and 400 m (bold) spacings.

3.3.1 Influence of measurement elevation

Figure 3.11A is a contour map of TMI computed at 12.5 m cell spacing and an elevation of 100 m above the top of magnetisation. This high-resolution proximal field provides rich information about the distribution of magnetisation. All anomalies would qualify as sweet-spots suitable for source depth estimation within the limitations of non-uniqueness previously discussed. The clusters of small adjacent bodies give rise to elevated background values where the anomalies overlap, but otherwise each of the 31 magnetisations is marked by an individual and reasonably separated anomaly that supports a depth estimate.

Figure 3.11B is a contour map of the field computed over the same magnetisation model at the same horizontal locations but at a higher elevation of 400 m above the top of magnetisation. In this case the 31 magnetisations give rise to only 14 closure peaks in the magnetic field. The clusters of smaller magnetisations each give rise to single anomalies, and the fields of several adjacent magnetisations merge into combined anomalies from which contributions from the individual sources cannot be reliably separated.

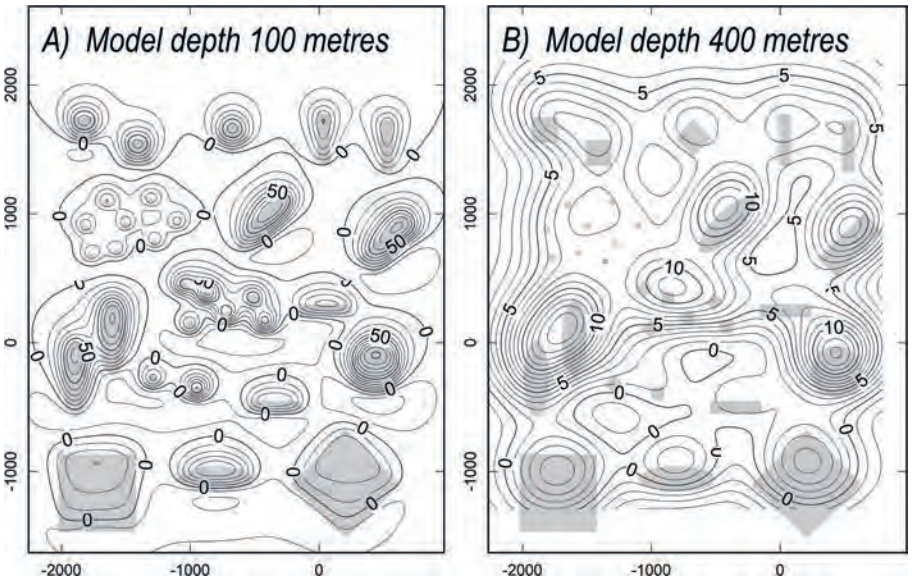

Fig. 3.11. A) TMI computed at 100 m elevation above magnetisation (contours at 5nT interval) and B) TMI computed at 400 m elevation (contours at 1 nT interval).

3.3.2 Complete survey multi-line inversion

Figure 3.12 shows the depth to the top of magnetisation values derived from inversion of the 400 m elevation, 100 m spaced flightline dataset after creating a starting model with individual bodies assigned to explain each of the recognised anomalies. The bodies are flat-topped (as were the bodies of the input model), have elliptic cross-section and are allowed to plunge (the input model bodies were all vertical). The inversion also introduces the freedom of a planar background field to represent uncertainty in making a regional separation (as encountered when working with field data). At most locations the field computed from the inversion model matches the input field very closely. Residual mismatches could be further reduced by introducing additional bodies or allowing additional complexity of the existing bodies but it is by no means clear than additional improvement in fitting the data would improve the validity in representing the input magnetisation. A statistical summary of the model is given in the top row (row 'A') of Table 3.1.

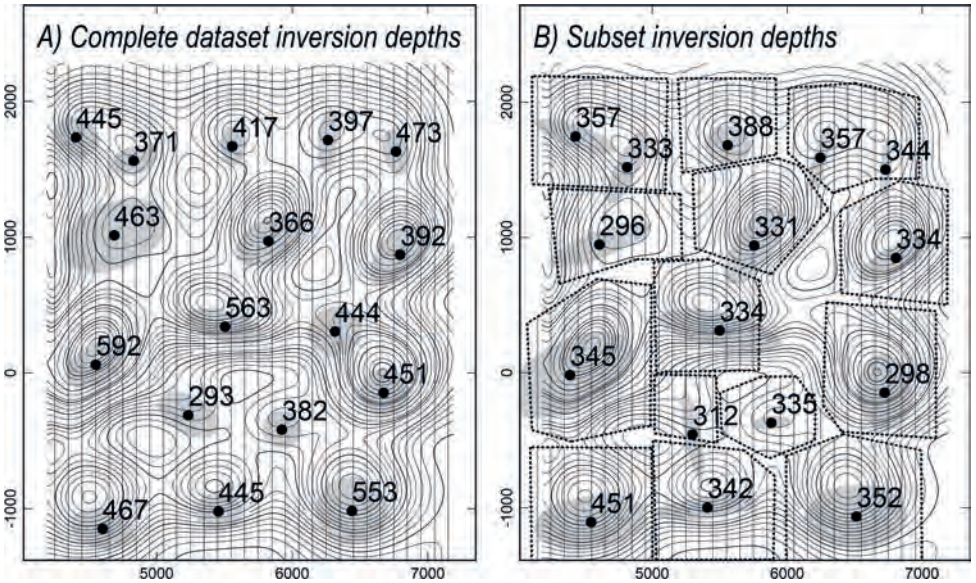

Fig. 3.12. Contours of TMI gridded from 100 m spaced flightlines (black) and of output inversion model field (dotted) with plan of the tops of the magnetisation models annotated with depth in metres. All input model depths are 400 m.

Table 3.1. Model depth-to-magnetisation estimates.

Inversion data	Spacing (m)	Number	Mean depth (m)	Std dev (m)	Min depth (m)	Max depth (m)
A) Complete lines	100	17	442 (+11%)	76 (19%)	293	592
B) Multi-lines	100	16	344 (–14%)	36 (9%)	296	451
C) Single lines	100	15	373(–7%)	39 (10%)	306	456
D) Computed traverses	–	14	400 (< 1%)	31 (8%)	351	473
E) Grid traverses	100	14	402 (+1%)	44 (11%)	336	480
F) Complete lines	400 odd	13	464 (+16%)	54 (14%)	370	550
G) Complete lines	400 even	14	454 (+14%)	119 (29%)	229	608
H) Multi-lines	400	11	416 (+4%)	113 (28%)	241	594
I) Single lines	400 odd	20	359 (–10%)	47 (12%)	284	456
J) Single lines	400 even	20	368 (–8%)	87 (22%)	243	572
K) Grid traverses	400 odd	12	374 (–7%)	68 (17%)	341	464
L) Grid traverses	400 even	13	316 (–21%)	63 (16%)	238	465

The mean depth to magnetisation is over-estimated by 11% and there is a standard deviation of almost 20% and maximum errors of -27% and +48% in the estimated depths. The details of this inversion model are poorly repeatable because there is trade-off between individual body parameters and between adjacent bodies, but the mean and standard deviation of the population of depth values remains consistent between repeat inversions. The smooth envelope of the least-squares best-fit field provides a general overestimation of depth, although there are also bodies of underestimated depth.

3.3.3 Multi-line single anomaly inversions

The inversion model shown in Fig. 3.12A is an attempt to best-fit the fields of all the magnetisations simultaneously, with weak focus on each and cross-compensation of errors between adjacent magnetisations. I also separately performed multi-line inversions of the individual anomalies. This method requires more work but better focuses the inversions by making only local adjustments of the magnetisation models to improve the local fit to the field above them. Where an anomaly appears to be due to multiple sources so close together that their fields cannot be separated, a compromise is made of performing a multi-body inversion for that complex anomaly. Results are shown in Fig. 3.12B.

As a starting model for each of these inversions I create an elliptic-section body with horizontal top and bottom faces and vertical sides. I assign a test magnetic susceptibility to the body and adjust the starting regional field to bring the sum of the regional and anomalous fields to an approximate match with the input field. A modest fit between the input field and that of the starting model is generally sufficient to ensure stable convergence of inversion. If the inversion does not proceed as intended it can be undone and the initial model, regional field or selection of free parameters can be adjusted to encourage different behaviour. I find this user guidance preferrable to 'hands-free' inversions that follow their own path, unbiased though that is. For these relatively simple inversions the only intervention required was to define the regional field and adjust it if required as the inversion progresses. The process of inversion, including any interpretive guidance or intervention, must be clearly documented so that the results can be fairly evaluated. The free model parameters in the inversion are the unknown values of magnetic susceptibility, easting and northing, depth, depth extent, axes lengths and dip. Adjustment of the regional can optionally be included in the inversion, or if preferred it can be kept fixed or can be adjusted by hand.

Statistics of the separate multi-line inversions are listed in the second row (row 'B') of Table 3.1. The main difference from the single inversion of the complete dataset is that depths are in most cases underestimated. Compared to the complete model inversion results the individual anomaly inversion depths have a reduced range of values and a standard deviation only one-half of that for the complete model inversion.

The inversion results listed in the two top rows of Table 3.1 suggest that the previously estimated uncertainty in recovered depth estimates of isolated simple geometry bodies of 5% to 10% due to fundamental non-uniqueness, increases to 10% to 15% if those

magnetisations are close to other surrounding unknown magnetisations. This loss of confidence in the depth values increases gradually from widely separated anomalies to anomalies with extensive overlap.

3.3.4 Single profile inversions

In section 3.2.2 I investigated depth estimation from single data profiles. Figure 3.13A shows the distribution of segments of flightlines selected for single-profile inversion of each anomaly. The main difference from multi-line inversions is that a single line inversion cannot obtain estimates of the strike length and azimuth of the magnetisation (because on a single line there is little sensitivity to those parameters). I first adjust the strike length and azimuth of the model in a map window to match the trend and strike extent of the anomaly and retain those settings throughout the inversion. Also, for inversion of a single profile it is generally more convenient to use a body of constant rectangular section unless there is a geological reason to prefer some other shape. Multi-line inversions allow freedom of movement of the horizontal reference coordinates of the magnetisation (most conveniently the centre of the top face). For single profile inversion there is little sensitivity to transition of the magnetisation in the across-profile direction. Therefore, horizontal displacement of the body is restricted to movement backwards or forwards along the profile (as if the body is moving along a track). The reference point need not be on the data profile if inspection of the grid suggests that the profile used is not centred over the magnetisation. For this example of closely spaced flightlines, displacements of the model centres from the selected lines are mostly small.

Single profile inversion simplifies data selection, reduces issues of complexity resulting from the horizontal shape and homogeneity of the magnetisation and focuses inversion on the more reliably defined, high-amplitude central sections of the anomalies. The single flightline inversion results are summarised in row C of Table 3.1. The range and standard deviation of the depth estimates are similar to the multi-profile inversion results but the error in mean depth is halved to 7% of total depth. Depth values are again generally underestimated.

3.3.5 Grid-traverse inversions

Another example of single profile inversion is the inversion of traverses through grids. Selection of grid traverses allows data to be extracted passing through anomaly maxima and minima parallel to the local field gradient. The quality of a grid in representing the magnetic field depends on the quality and distribution of the primary data, the variation patterns of the true magnetic field and the interpolation algorithm used. There is also degradation of data in resampling from the grid to a

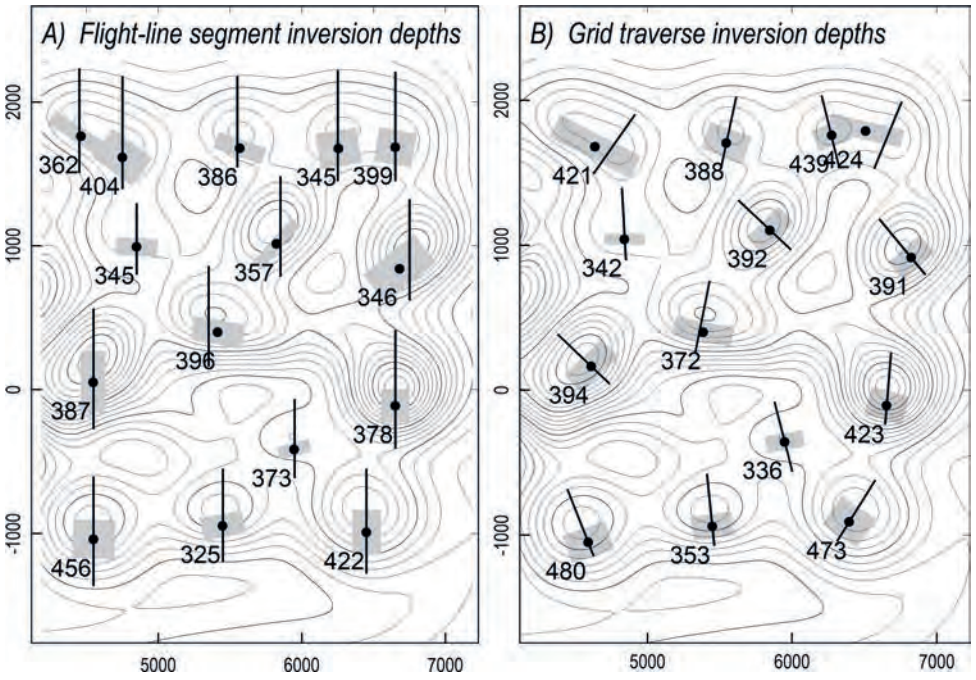

Fig. 3.13. Magnetisation depth 400 m, line spacing 100 m. TMI contours with A) inverted flightline segments and B) inverted grid traverses. Annotations are depths to top of magnetisation in metres.

traverse through it, unless those traverses are along grid rows or columns. To objectively investigate inversion of grid data I used an automated algorithm to draw traverses through each grid peak in the direction of maximum gradient. These grid traverses are shown in Fig. 3.13B. To provide a reference against which to evaluate the influence of gridding I also directly computed the magnetic field along the traverses. Statistics of the depth estimates from inversions of these directly computed traverses are listed in row D of Table 3.1. There is a low error in the mean depth value and the standard deviation and range of the depth solutions are similar to those for the single flightline inversions (as should be expected because both datasets are directly computed from the same input model). The models and annotated depth values shown in Fig. 3.13B are from individual inversions of the gridded data interpolated along the traverses. The results are listed in row E of Table 3.1. For this grid created from adequate sampling of close line-spaced data there is only a 1% error in the mean depth estimate. The standard deviation and range of the solutions are 11% and 36% respectively. These values are similar to those for solutions from inversion of the directly computed data traverses (we will see that this is in contrast to traverses through grids generated from an insufficient line spacing).

3.3.6 Under sampling of the magnetic field

In this section I investigate how inversion of multiple flightlines, single flightlines and grid traverses performs for an insufficient sampling of a magnetic field defined from flightlines at 400 m spacing (equal to the depth to the top of magnetisation). Each of the 400 m spaced flight lines is identical to a line in the 100 m spaced set, the difference is the absence of three-quarters of the lines. Following the rules of Reid (1980) this is an inadequate representation of the magnetic field for inversion or depth estimation. The line data are valid but at the wide line spacing do not reliably map the magnetic field. Some anomalies are not sampled by this wider line spacing and some separations between adjacent anomalies are not sampled, creating fewer, larger anomalies. Under-sampling of the field in some cases misses areas of sharp gradient that are most diagnostic of how deep a source is, encouraging overestimation of depth. However, in some cases under-sampling also causes misrepresentations that give rise to underestimation of depth.

Where significant differences between grids derived from subsets of survey lines (e.g. between sets of alternate odd- and even-numbered survey flightlines) reveals that those subsets insufficiently sample the magnetic field there is concern that their combination may also under sample the field. Figures 3.14A and 3.14B show

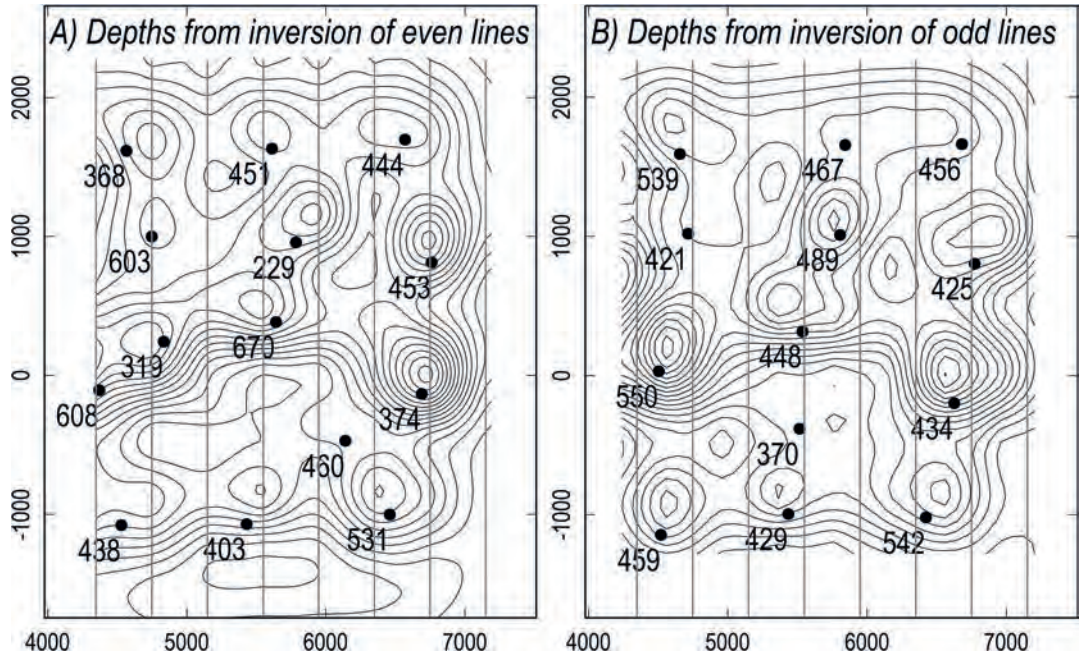

Fig. 3.14. TMI contours and annotated depths (in metres) to magnetisation derived from inversion of two 400 m spaced line sets A) and B) with a 200 m displacement between them.

contours of grids produced from two sets of 400 m spaced flightlines displaced from each other by 200 m, together with the annotated depth estimates from inversion of each subset of lines (these values can be compared to inversion of the complete 100 m spaced line set shown in Fig. 3.12A). Inversion produces 13 source models from inversion of one dataset and 14 from the other. There are 11 pairs of solutions for the same (but differently sampled) anomalies. Of those 11 pairs, seven have depth values within 10% of each other but there are also other pairs with differences of over 50%. There are also some substantial horizontal displacements between the centres of bodies derived from the two inversions. Statistics of the depth values are listed in rows F and G of Table 3.1. The average depth values for the two inversions are overestimated by 15% and the mean standard deviation is 22%.

3.3.7 Under-sampled survey multi-line anomaly inversions

For inversion of the 100 m line-spaced data there was an improvement of the depth estimates derived from single-anomaly, multi-line inversions rather than from simultaneous inversion of the complete dataset. For the 400 m line-spaced data there are few anomalies suitably sampled for individual multi-line inversion. In a compromise the data were divided into subsets of overlapping anomalies. The inversion depths are listed in row H of Table 3.1. The mean depth error is significantly reduced from simultaneous inversion of the complete dataset but the standard deviation and range of values is similar.

3.3.8 Under-sampled survey single profile inversions

Single flightline inversions also suffer from under-sampling of the magnetic field because critical segments of the field that would have been more suitable for depth estimation may not be measured and because the horizontal centre location and horizontal extents of the magnetisations are misrepresented by the under-sampling. Flightline segments for single-line inversion were selected from both sets of 400 m spaced lines. Figures 3.15A and 3.15B show segments of the flightlines selected for individual inversion of each anomaly, together with centre points of the inversion models and their annotated depth values. Many of the anomalies are centred on profiles, because at a wide line spacing individual anomalies may have strong expression on only one profile. Just as for the complete dataset inversions, there is reasonable agreement between many of the pairs of depths from the even and odd alternate line samplings. Statistics of the depth values are listed in rows I and J of Table 3.1. There is a mean underestimation of depth by ~10% for each of the sets of depths.

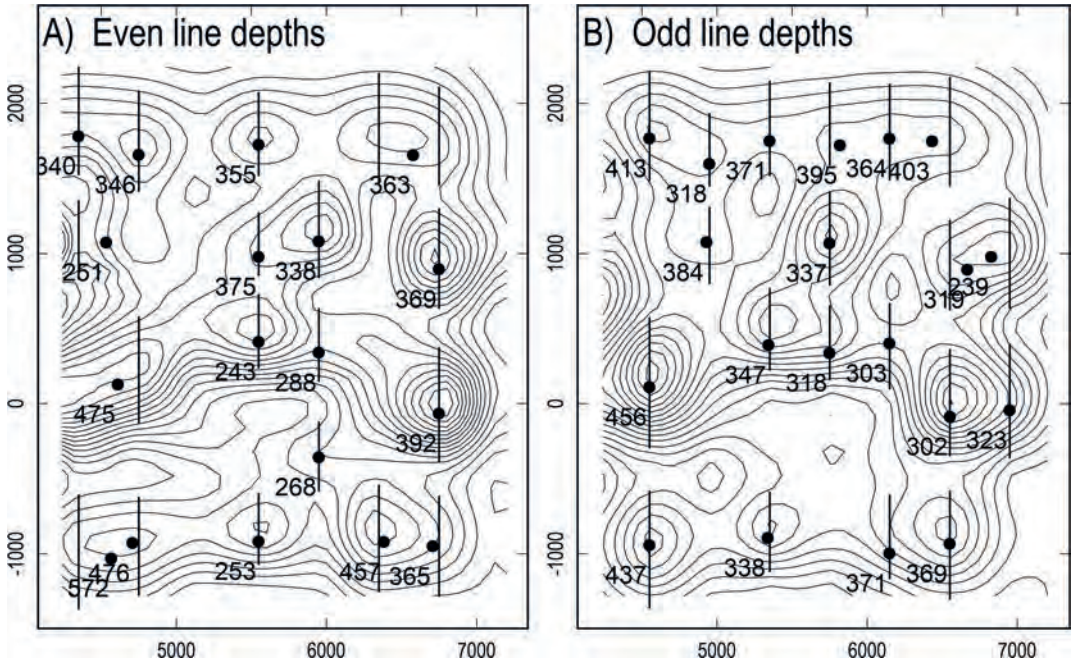

Fig. 3.15. TMI Contours and annotated model depths from inversion of segments of the 200 m displaced sets A) and B) of 400 m spaced flightlines with the annotated depths in metres.

3.3.9 Under-sampled survey grid-traverse inversions

Grid traverses derived from the 100 m and the 400 m line-spaced data are quite different to each other. For the 100 m spaced line data the gridded TMI interpolated onto traverses through the grid maxima is similar to TMI directly computed along those lines from the input model. However, on traverses through grids of the 400 m spaced flightlines there are substantial differences between the directly computed data and data interpolated from the grid, as shown in Fig. 3.16. This reveals substantial inadequacy in gridding of widely spaced data to represent the true magnetic field variation. Significant horizontal shifts between peaks of the directly computed and grid-interpolated channels show that in many cases the TMI grid mis-locates the magnetisations, and significant differences in curvature of the channels gives rise to errors in estimation of magnetisation depths.

Figure 3.17 shows the tracks of grid traverses automatically generated through maxima of the two grids of 400 m line-spaced data with annotated depth estimates from inversion of the grid data interpolated onto those traverses. Statistics of the depth values are listed in rows K and L of Table 3.1. Few of the depth values are correctly centred on the input model magnetisations and more plot off the magnetisation bodies than over them. Just as for the individual flightline segment inversions, the solutions are mostly underestimates of depth.

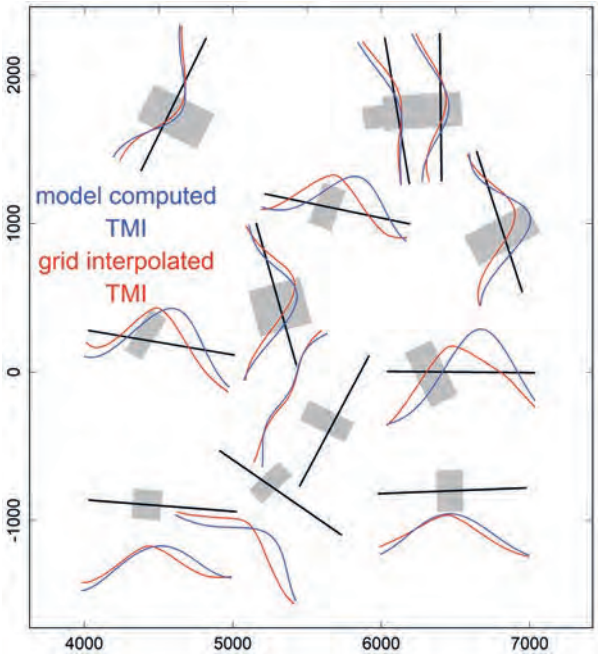

Fig. 3.16. Stacked profiles of the model field computed along the grid traverses (blue) and the field interpolated from gridding of the 400 m line-spaced data (red) with a plan view of the top of the inversion model bodies.

3.3.10 Conclusions of the synthetic data inversion study

This synthetic, noise-free study has established several key issues for estimation of depth-to-magnetisation:

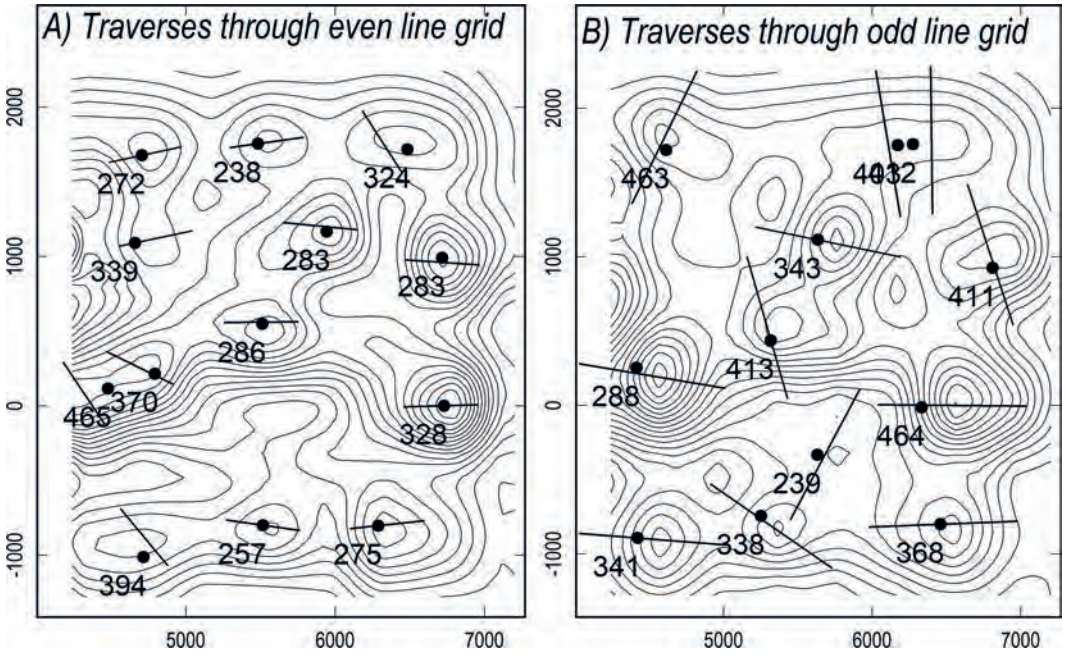

Fig. 3.17. Traverses and annotated depths (metres) from grid-traverse inversions of the two 400 m line-spaced grids.

1) Fundamental non-uniqueness resulting from unknown values of magnetic susceptibility, shape and size restricts confidence in depth-to-magnetisation estimates from isolated, well-defined anomalies to no better than 5%.
2) Anomaly isolation is a key source of additional uncertainty.
3) Individual focus on single anomalies provides superior depth estimates.
4) Field curvature is the most reliable indication of depth-to-magnetisation and is best estimated on well chosen individual profiles – ideally profiles of direct measurements.
5) Fidelity of field curvature is difficult to preserve in gridding – particularly of widely spaced data and this restricts reliability of depth estimates made from gridded data.

3.4 A DEPTH TO MAGNETISATION FIELD STUDY OF SEDAN, SOUTH AUSTRALIA

The Sedan detailed aeromagnetic survey (location shown in Fig. 3.18) was flown over an area with basement rocks belonging to the Delamerian Orogeny which include Cambrian-Ordovician mafic to felsic intrusives with some minor Cambrian metasediments. This basement is overlain by up to 100 m of weakly magnetic Tertiary cover. The shallowest strong magnetisation is expected to be at the top of fresh basement beneath a deep and variable weathering of the pre-Tertiary surface. The igneous rocks that source the highest amplitude magnetic field variations are a suite of complex, zoned intrusions with high magnetisation in the more mafic zones and moderate to low magnetisation in the more granitic zones. In 1999 the Geological Survey of South Australia commissioned a regional aeromagnetic survey over the Sedan area. This survey (referred to here as the regional survey) was flown on east–west flightlines at a line spacing of 400 m and nominal terrain clearance of 80 m. At the same time the contractor flew a more detailed survey of a mineral tenement within the area. This survey (referred to here as the detailed survey) was flown on east–west flightlines at a line spacing of 80 m and nominal terrain clearance of 50 m. The two surveys were managed so that the regional survey flight and tie lines are horizontally coincident with detailed survey lines. Flightline maps of the two surveys are shown in Fig. 3.19.

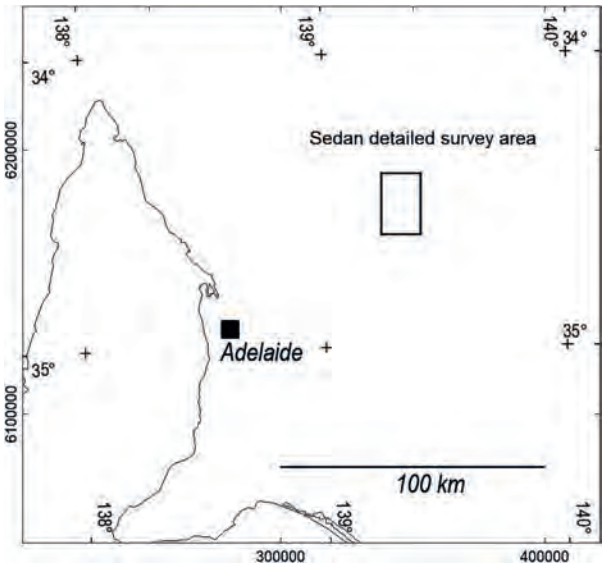

Fig. 3.18. Location of the Sedan detailed survey area.

There is a moderate variation in ground elevation of 160 m across the area and the range in TMI is ~1,200 nT. The two surveys provide a rare opportunity to compare data at different line spacings and elevations flown with the same aircraft, instruments and pilot and with the data processed identically. There are too few drill intersections of magnetisation to provide a meaningful ground-truthing of depths predicted from analysis and interpretation of the magnetic field data but nevertheless, these two surveys provide a test of the predictions of the previous synthetic data study. TMI images from gridding of each survey dataset are plotted in Fig. 3.20. Both TMI images show similar general features, with greater detail resolved by the closer line-spaced survey. Figure 3.21 shows very similar TMI profiles from the detailed and regional surveys along a horizontally coincident north–south tie-line (for location see Fig. 3.20). The short wavelength variations are of slightly higher amplitude in the lower elevation detailed survey than in the regional survey but this difference is almost removed by upward continuation of the detailed survey measurements by the average difference in reported elevation for the two lines of 24 m. Minor remaining long-wavelength differences between the two datasets may be due to differences in levelling of the data and/or along-profile variations of sensor elevation. Three sub-areas are outlined in Figs 3.19 and 3.20 for more detailed investigation.

Typical data complexity issues are illustrated in Fig. 3.22. The magnetometer elevation and horizontal position were monitored with global positioning system (GPS) instruments using real-time differential correction. There are variations in GPS elevation with

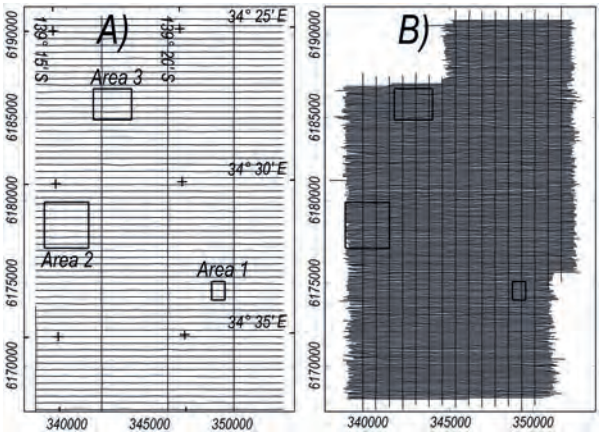

Fig. 3.19. Flight plans of A) the regional survey and B) the detailed survey.

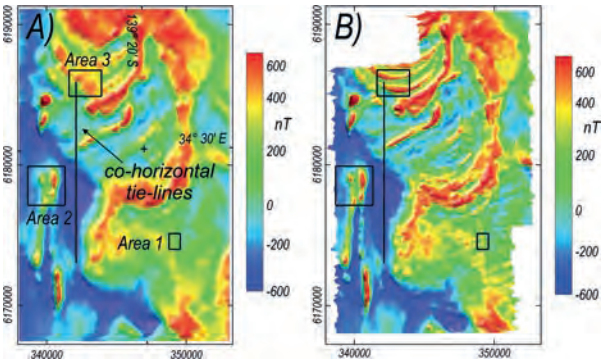

Fig. 3.20. TMI images from the regional survey (left) and detailed survey (right).

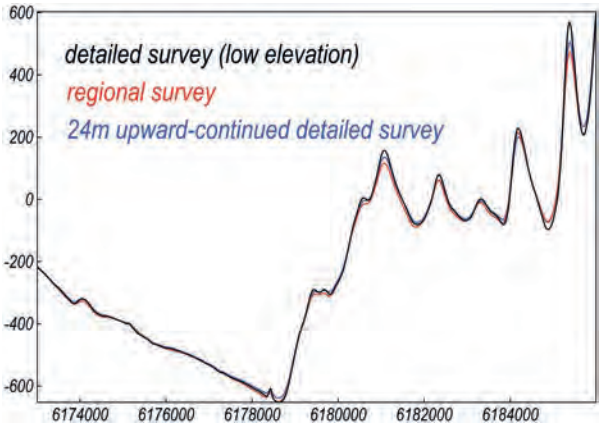

Fig. 3.21. Coincident regional and detailed survey N-S flightline TMI profiles (length 13 km -for location see Fig. 3.29).

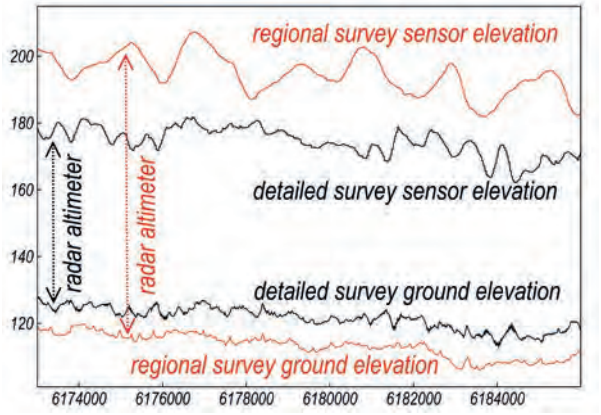

Fig. 3.22. Coincident regional and detailed survey N-S flightline GPS altimeter and DEM profiles (length 13 km – for location see Fig. 3.29).

wavelengths of up to 2 km and amplitudes up to 10 m in the detailed survey data and up to 15 m in the regional survey data that are uncorrelated between the surveys. Ideally use of the GPS channel provides compensation for these elevation differences in magnetic field computations, but exact linkage between the magnetic field and elevation is not preserved in the network adjustment (levelling) of the data. The surveys also measured elevation of the aircraft above the ground surface using a radar altimeter. Subtraction of the radar altimeter from the GPS altimeter should map the ground surface elevation. A digital elevation model (dem) of the ground surface is published as both a line data channel and a grid in the contractor-supplied survey data. An example of the line data is plotted in Fig. 3.22. The dem channels from the two surveys show common low-amplitude, long-wavelength variation and uncorrelated shorter wavelength variations of up to 5 m amplitude. However, the most prominent feature is the 8 m displacement between the curves which should be coincident. This is most likely due to improper calibration of the radar altimeter, which is disappointing as the same instrument was used in the two surveys. Given that a primary objective of the detailed magnetic field survey is to map depth-to-magnetisation beneath the ground surface, the starting point of an inconsistency of 8 m between these survey datasets clearly adds to uncertainty in the subsequent estimate of depth to magnetisation below that surface.

3.4.1 Area 1

Figure 3.23 shows regional and detailed survey TMI images over Area 1 (for context see Fig. 3.20). The image colour scales are similar and the contour interval for both images is 20 nT. The centre of the detailed survey is dominated by a prominent anomaly of c. 100 nT peak

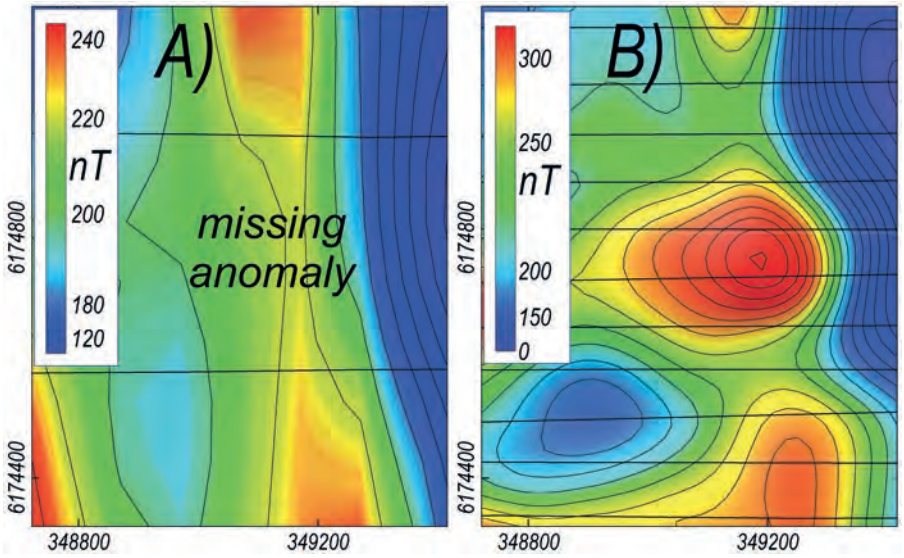

Fig. 3.23. TMI images of Area 1 (for location see Figs 3.19 and 3.20) from A) the regional survey and B) the detailed survey. For both images the contour interval is 20 nT.

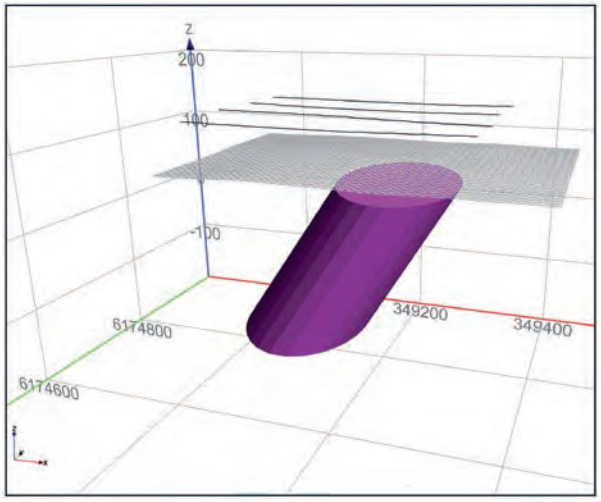

Fig. 3.24. Perspective of inversion model and flightlines.

amplitude. Two flightlines pass through the centre of this anomaly with the peak apparently halfway between them (Fig. 3.23B). The two adjacent lines to north and south define the flanks of the anomaly which has a north–south width of ~240 m. The anomaly is not evident in the regional survey because it is centred halfway between regional survey lines at 400 m spacing (Fig. 3.23A). A model generated from inversion of a segment of five detailed survey flightlines is shown in Fig. 3.24. The field computed from the model closely matches the measured field. The modelled top of magnetisation is 39 m below the ground surface and 89 m below the mean sensor elevation. The magnetisation appears to have roughly circular cross-section with a diameter of just over 200 m, a depth extent of 180 m and a volume of over 5×10^6 m^3.

The detailed survey anomaly is sufficiently defined to estimate a magnetisation direction. The best estimated magnetisation has intensity 0.9 A/m, declination 195° and inclination −69°. This direction is rotated from the local geomagnetic field direction by 44° which is a confident indication that remanent magnetisation is significant. Clearly none of this information can be recovered from the regional survey data.

This example indicates the inadequacy of wide line spacing for mapping shallow magnetisations of small extent. Anomalies of this size and shape might be of economic significance (e.g. diamondiferous kimberlite pipes) and if those were targets of interest the regional survey would be unreliable for finding them. If the regional survey had been flown with a 200 m north–south shift one of the flightlines would have passed over the anomaly and clearly detected it, but interpretation would still be difficult because it would be defined only on that single line. Regional 400 m line-spaced surveys have been flown over large areas in Australia. To investigate small but potentially significant anomalies detected by these surveys on only single flight lines there is a case for dedicated drone surveys that can detail the anomalies at low elevation and much closer line spacing. At lower elevation, shallow magnetisations produce significantly higher-amplitude anomalies allowing them to be mapped without the same precision required

of aeromagnetic surveys to map low-amplitude field variations over large parts of their survey area. Another method to improve data coverage is to use cross-line, wing-tip gradiometry. Gradiometry would not have solved this example of extreme insufficiency in mapping magnetisation but it provides valuable additional information for less problematic cases of inadequate sampling. Unfortunately, increased cost of wing-tip gradiometry is commonly offset against flying surveys at wider line-spacing, in large part negating the potential advantage of the data.

3.4.2 Area 2 complete dataset inversions

Figure 3.25A shows TMI mapped from the regional survey data in Area 2 (see Fig. 3.20 for location). The anomalies are elongated, partially overlap and are aligned north–south perpendicular to the east–west flightlines. A corresponding image of TMI forward computed from an inversion model of the data is shown in Fig. 3.25B. The close match of measured and model computed fields suggests that this model is at least a candidate representation of the ground magnetisation, but in the previous synthetic data study similarly close data-fits were achieved by models with error in estimated depth of over 10%. This model of a geological magnetisation derived from measured data is likely to have more substantial failings. The values posted in Fig. 3.25B are estimated elevations of the top of magnetisation in metres below sea level. The datum is determined by referencing elevation to the GPS altimeter measurements. For each of the anomalies labelled in Fig. 3.25A the depth-to-magnetisation statistics are listed in Table 3.2 and summarised in Table 3.3. In the synthetic data study the top of magnetisation was at a constant elevation and the scatter of values was due completely to errors in the depth estimation. For this study the elevation of each magnetisation is unknown and is likely to vary between anomalies, so the range of estimated depth values is an unknown mixture of true depth variation between different magnetisations and errors in estimation of those values. For the five selected anomalies the mean elevation is 94 m BSL, the mean depth below sensor is 327 m and the mean depth below ground is 247 m, with a range of 148 m.

Figure 3.26A shows the TMI image over the same area generated from the detailed survey data, and Fig. 3.26B shows a matching TMI image forward computed from the model derived from inversion of that data. For the five selected anomalies the mean elevation is 89 m BSL, the mean depth below sensor is 283 m and the mean depth below ground is 233 m with a range of 71 m. Multi-flightline inversions of the two survey datasets provide consistent results. The difference between the mean elevation of the five anomaly source models from inversion of the two survey datasets is only 5 m, and the difference in their mean depths below ground is only 14 m (Table 3.3) that is 5% of the average depth below sensor. The average difference between corresponding pairs of estimates of depth to magnetisation below ground is 25 m (9% of the average depth below sensor).

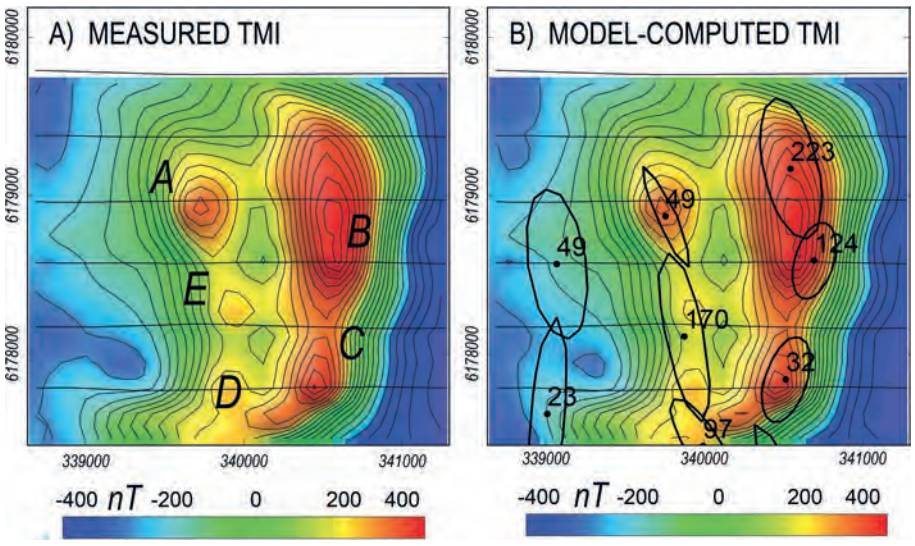

Fig. 3.25. Area 2 Regional survey A) measured TMI and B) TMI computed from the inversion model with body plan and annotated top of magnetisation elevation (metres BSL).

Table 3.2. Sedan Area 2 summary of depth to top of inversion models.

Survey	Data	Susceptibility (SI)	Top elevation (m ASL)	Sensor (m ASL)	Ground (m ASL)	Depth below ground (m)	Depth below sensor (m)
Anomaly_A							
regional	complete	0.336	–49	240	160	209	289
regional	traverse	.0872	68	229	149	81	161
regional	flightline	.137	55	234	146	91	179
detailed	complete	.342	–48	198	148	196	246
detailed	traverse	.535	14	208	158	144	194
detailed	flightline	.124	61	210	157	96	149
Anomaly_B							
regional	complete	0.621	–124	224	144	268	348
regional	traverse	.161	–75	213	133	208	288
regional	flightline	.211	–90	215	132	222	305
detailed	complete	.354	–110	181	131	241	291
detailed	traverse	.187	–16	191	141	157	207
detailed	flightline	.286	–37	191	142	179	228
Anomaly_C							
regional	complete	0.266	–32	227	147	179	259
regional	traverse	.572	99	225	145	46	126
regional	flightline	.189	9	207	141	132	198
detailed	complete	.509	–61	195	145	206	256
detailed	traverse	.291	33	195	145	112	162
detailed	flightline	.138	56	194	145	89	138
Anomaly_D							
regional	complete	0.356	–97	236	156	253	333
regional	traverse	.0443	46	229	149	103	183
regional	flightline	.156	15	228	149	134	213
detailed	complete	.377	–118	199	149	267	317
detailed	traverse	.195	14	202	152	138	188
detailed	flightline	.163	5	204	153	148	199
Anomaly_E							
regional	complete	0.256	–170	237	157	327	407
regional	traverse	.0942	68	228	148	80	160
regional	flightline	.0194	106	231	146	40	125
detailed	complete	.385	–107	197	147	254	304
detailed	traverse	.0848	10	205	155	145	195
detailed	flightline	.107	50	209	155	105	159

In the Sedan area the weak magnetisation contrast across the ground surface does not generate significant magnetic field variations in the aeromagnetic data (the ground is magnetically 'transparent') and performance of the magnetic source depth analysis is most appropriately referenced to depth below sensor. However, to users of the depth estimates the most relevant measure is depth below ground. Accumulation of uncertainty as a percentage of depth from the sensor to the ground surface is effectively a penalty for aeromagnetic data. For the Sedan surveys flown at nominal elevations of 80 and 50 m above the ground and with the top of magnetisation

Table 3.3. Summary of Area 2 depth-below-ground estimates.

Survey	Data	Mean depth (metres)	Samples	
regional	complete lines	247	5	
detailed	complete lines	233	5	
regional	grid-traverse	104	5	
detailed	grid-traverse	139	5	
regional	Single flightline	124	5	
detailed	Single flightline	123	5	
Differences between results				**Standard deviation (metres)**
regional-detailed	complete line set inversions	25	5	23
regional-detailed	grid-traverse inversions	56	5	13
regional-detailed	single flightline inversions	34	5	24
regional	grid-traverse and flightline inversions	36	5	30
detailed	grid-traverse and flightline inversions	29	5	15

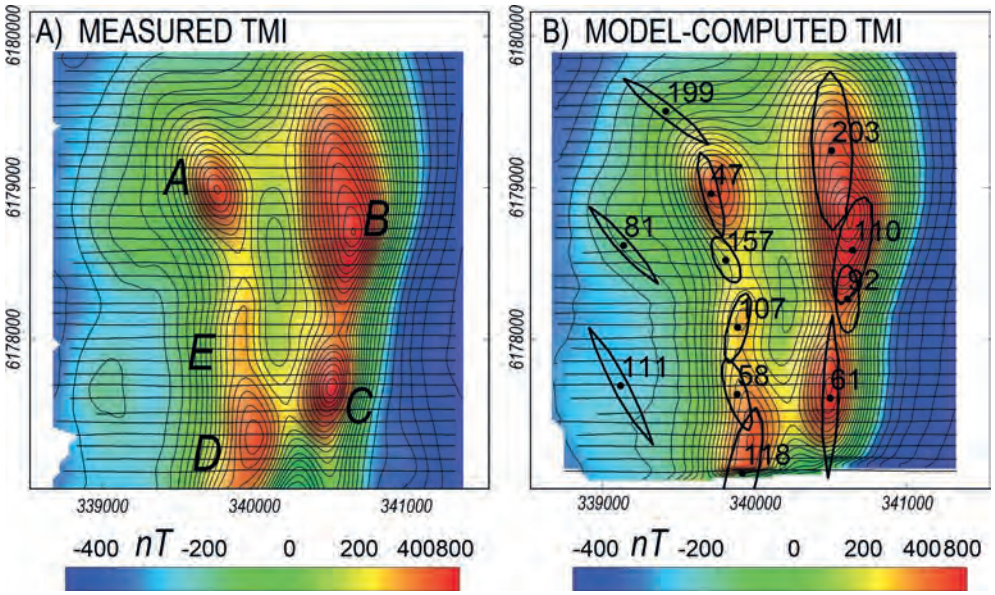

Fig. 3.26. Area 2 Detailed survey A) measured TMI and B) TMI computed from the inversion model with body plan and annotated top of magnetisation elevation (metres BSL).

in most places more than 100 m below ground this penalty is not prohibitive, but for substantially shallower magnetisations or greater flying heights the uncertainty accumulated between the sensor elevation and the ground surface can exceed the average depth of magnetisation below surface. In such cases depth-below-ground estimates generated from aeromagnetic data analysis have little meaning. For depths that must be known reliably (e.g. as a basis for making drilling decisions) a lower elevation or ground surface survey should be acquired to upgrade the aeromagnetic analysis results.

3.4.3 Area 2 single flightline and grid-traverse inversions

In the synthetic data study the most reliable depth-to-magnetisation estimates were derived from inversions of carefully selected segments of single flightlines. A corresponding example from the study of area 2 is shown in Fig. 3.27. In this example there is a subtle inflection on the western flank of the anomaly that is unlikely to be recognised as significant in a grid traverse (although the feature can just be seen as a minor bulge in the grid contours in Fig. 3.26A). This feature is

confirmed more clearly in the upper vertical derivative track. This track is derived from FFT analysis of the closely spaced and directly measured flight line data. The transform is approximate because there are no estimates of the cross-line horizontal gradients, but those are relatively weak and the transform applied identically to the measured and model computed fields allows valid comparison in optimising the inversion with reduced concern for the regional field separation and the depth extent of the bodies. The main function of the weakly magnetised western body is to allow the more prominent easterly magnetisation to explain only the main anomaly. After inversion, the western body can optionally be retained or discarded. Individual profile inversion depths for the various anomalies derived from both the regional and detailed surveys are listed in Table 3.2.

Figure 3.28 shows an example south-east to north-west grid traverse through the detailed grid anomalies C and E. There is overlap between the flanks of the anomalies but this does not substantially change the sharpness of curvature over their centres and therefore has little impact on the depth-to-magnetisation estimates. The overlap does, however, introduce an opportunity to incorrectly assign overlapping field variations between the two magnetisations and change the asymmetry of each anomaly from which the apparent dip of the magnetised bodies is estimated. For both the flightline and grid-traverse inversions the field variation assigned to the regional might include contributions from deep extensions of the magnetisations, but this has little effect in estimation of depths to their tops. Figure 3.28 also shows the location and profile intersection of bodies derived from inversion of the adjacent Traverse C

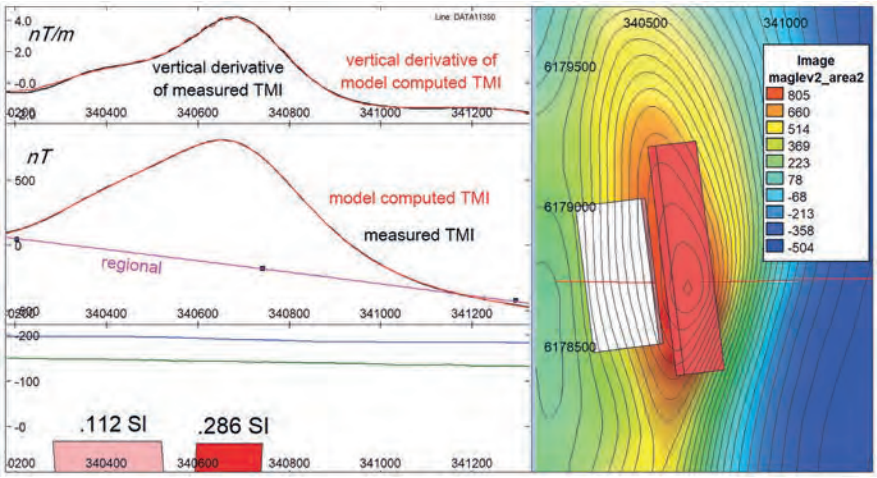

Fig. 3.27. Detailed survey flightline inversion through anomaly B in area 2 (for location see Fig. 3.26A).

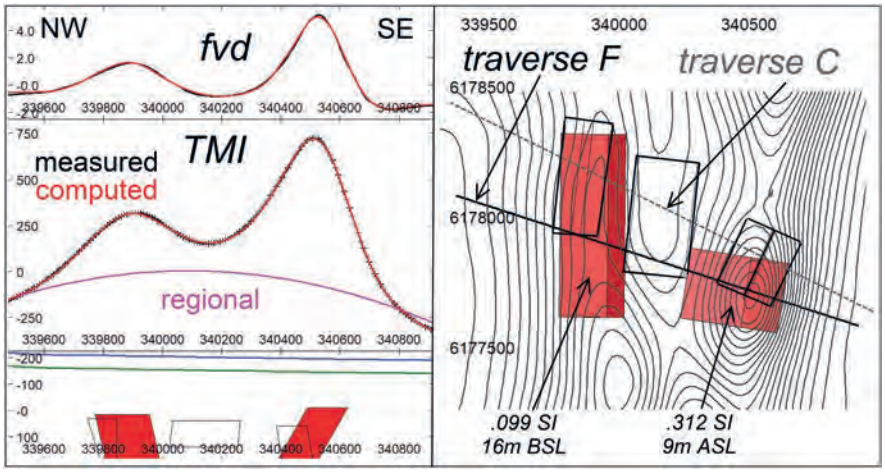

Fig. 3.28. Detailed survey flightline inversion through anomalies C and E in area 2 (for location see Fig. 3.26A).

through the regional survey grid. The two survey grids are representations of the same magnetic field (with a difference in elevation between them of 30 m) but as a result of the different sampling the two grids are best interrogated on differently located traverses. Tops of the detailed grid-traverse inversion bodies shown in red in Fig. 3.28 are both shallower than tops of the corresponding regional survey grid-traverse bodies (shown in outline).

As reported in Table 3.3, the mean grid-traverse depth below ground estimate from inversion of the regional survey data is shallower than the estimate from the complete-dataset regional survey inversion (104 m compared to 247 m) consistent with relationships established in the synthetic data study. The same relationship (but with a smaller discrepancy) is seen for the mean depths of the detailed survey inversions (139 m for the grid-traverses compared to 233 m for the complete dataset). From learnings of the synthetic data study the individual flightline segment inversions are considered the most reliable depths and these show little variation in mean values between the two surveys.

Relationships between depths derived by the various methods are also summarised in Fig. 3.29. Consistent with the results of the synthetic data study, the regional and detailed survey complete-dataset inversion depth-below-ground values (plotted in black in Fig. 3.29) are significantly deeper than the sweet-spot individual grid-traverse and single flightline inversion depths (plotted in red and blue). The detailed and regional survey single flightline inversion depths (red and blue crosses respectively) have almost identical mean values of 123 and 124 m but the mean grid-traverse depths for the two surveys differ by 35 m (139 and 104 m). Many of the cross-plotted

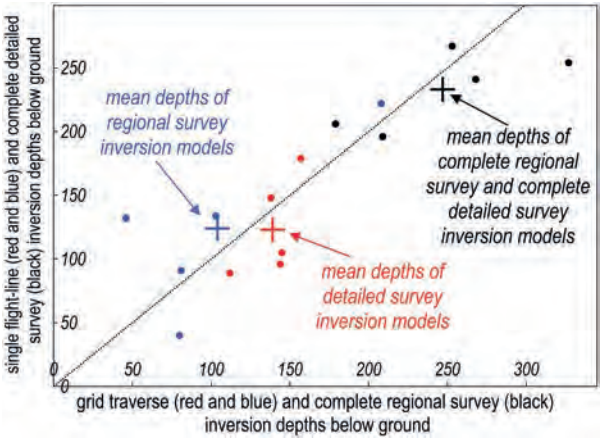

Fig. 3.29. Cross-plots of depth estimates in Area 2 derived from the two surveys and different data types.

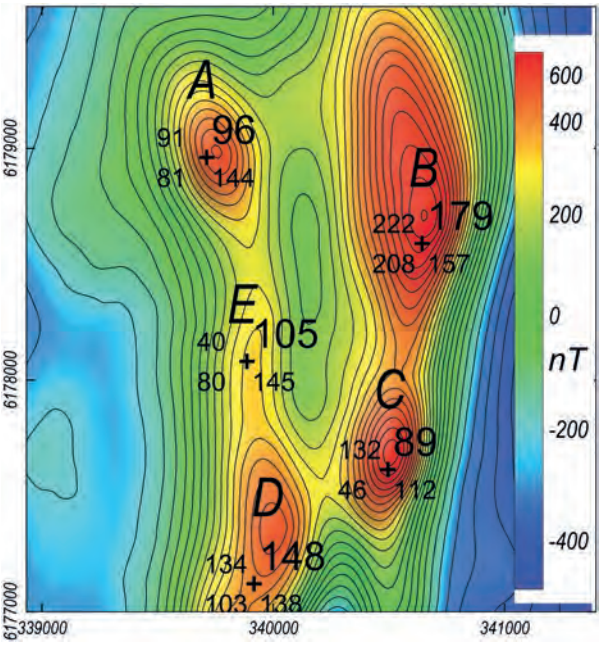

Fig. 3.30. Depth-below-ground estimates for each anomaly. The upper values are from the detailed survey and lower values from the regional survey. Left-hand values are from grid traverses and right-hand values are from flightlines. The bold upper right values from inversion of detailed survey flightline data are the preferred depths.

individual depth values are close to the 1:1 slope and hopefully the variations along that line are substantially due to true depth variation to the source of each anomaly. From lessons learnt in the synthetic data study the preferred depth values are those derived by single flightline inversions of the detailed survey data.

Individual grid-traverse and single flightline depth values for each anomaly are mapped in Fig. 3.30. The best estimate of mean depth below sensor is 175 m for the detailed survey and 204 m for the regional survey. For the flightline spacings of 80 m and 400 m this gives line spacing to source depth ratios of 1:2.2 and 1: 0.5 for the detailed and regional surveys respectively. This is a less satisfactory sampling of the magnetic field than was investigated in the synthetic data study and would be expected to give larger proportional depth errors. However, for this section of the Sedan survey the anomalies are elongate perpendicular to the flightline direction and this optimises fidelity with which depth estimates are recovered.

3.4.4 Area 3 regional and detailed survey TMI anomalies

Figure 3.31 shows TMI images from Area 3 (for location see Fig. 3.20). For Area 2 the TMI images of the regional

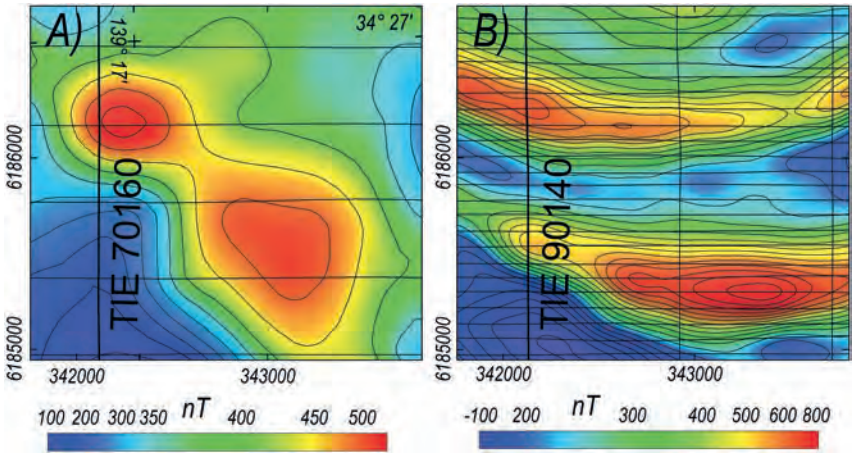

Fig. 3.31. Area 3 TMI and flight lines: A) regional survey and B) detailed survey.

and detailed surveys were broadly similar. For Area 3 it is difficult to recognise that the two TMI images are of the same area. Under-sampling at the 400 m line spacing of the regional survey completely distorts representation of the magnetic field. The anomalies in Area 3 are more elongate than those in Area 2 which should provide advantage in mapping the magnetic field. However, in Area 3 elongation of the anomalies is almost parallel to the flightline direction rather than perpendicular to it as in Area 2. Figure 3.32 shows a 2.3 km section of a horizontally co-located north–south tie-line with data from both surveys. The northern and southern anomalies in the detailed survey data have amplitudes of 450 and 410 nT respectively. Those peak values are smaller by 40 and 95 nT respectively for the regional survey measurements made at a higher elevation. A substantial part of this difference is removed by applying a 23.4 m upward continuation filter to the detailed survey data to compensate for the reported mean elevation difference between the profiles. The remaining differences between the profiles reduced to the same elevation are primarily long wavelength variations due to differences in elevation along the individual profiles or introduced in the two different survey network adjustments of the data. However, these longer wavelength differences do not significantly influence the local curvature of the field at the peaks of the anomalies and have little effect on the depth estimates.

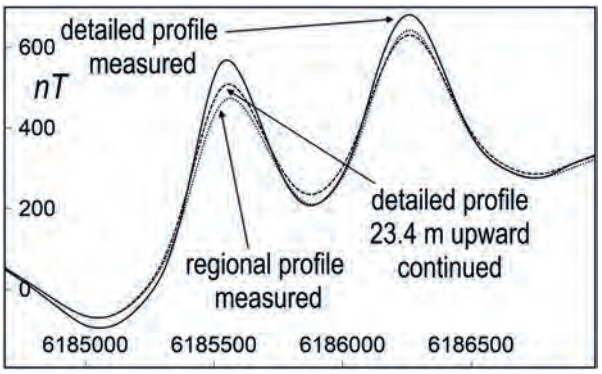

Fig. 3.32. TMI on a coincident regional and detailed survey flightline (located in Fig. 3.31).

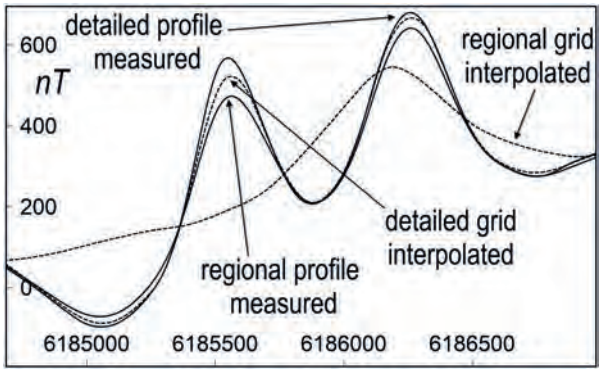

Fig. 3.33. TMI on a coincident regional and detailed survey tie-line (located in Fig. 3.31).

Figure 3.33 also shows measured TMI along the profile, in this case together with interpolation of the regional and detailed TMI grids. The algorithm used in gridding both survey datasets ensures that the grid values along the flightlines approximately honour the profile data. However, tie-lines are discarded once they have been used for network adjustment and are not directly included in the gridding. The detailed survey grid interpolation reasonably matches the measured tie-line data from that survey with minor attenuation of the shorter wavelength anomalies (their peak to trough amplitudes are reduced slightly). However, as shown in

Fig. 3.33, for the regional survey the data interpolated from that grid onto the tie-line completely misrepresents the directly measured data. The segment of the regional survey tie-line in Fig. 3.33 includes only five survey flightline intersections to provide samples for generation of the grid. The regional survey TMI grid interpolation does not reveal the southern anomaly at all and the northern anomaly is much broader, of lower amplitude and horizontally displaced relative to the profile measurements. Clearly no depth can be estimated from the interpolated regional survey grid data for the missing southern anomaly and any depth estimate for the northern anomaly will be highly erroneous. In Fig. 3.31 the catastrophic under-sampling of the magnetic field by the regional survey grid is obvious by comparison with the detailed survey grid. The only evidence of that under-sampling from the regional survey data itself is the discrepancy between the measured and grid-interpolated data along the tie-line as shown in Fig. 3.33. Very few users of grid data interrogate the validity of a grid in this way and consequently significant deficiencies in grids go undetected. Any grid-based methods of depth estimation will only provide misleading results from this segment of the regional survey grid and second order derivatives of the gridded data as used in some depth estimation methods are completely fictitious.

3.4.5 Area 3 individual grid-traverse and single tie-line segment inversions

Inversion of single measured profiles in Area 3 from either survey is restricted to the tie-lines because the flight lines are too oblique to the field variations for individual analysis or inversion. Figure 3.34 shows inversion of a tie-line from the detailed survey. Also shown for comparison is the intersection of the model from inversion of a coincident (but higher) regional survey line. The models are in excellent agreement. In a total depth below sensor of over 200 m there is only a 13 m difference in depth between the tops of the southern magnetisation models (the detailed survey inversion gives the shallower result). As predicted from the synthetic data study, in compensation for the difference in depth the deeper body is narrower and of higher apparent susceptibility. Depth to magnetisation is well mapped at the tie-line intersections with the northern and southern anomalies but even for the detailed survey these tie-line intersections only occur at 800 m intervals. Any attempt to estimate depth to magnetisation from grid data in Area 3 is poorly justified. The quality of depth estimates can be improved for these linear anomalies by use of anisotropic gridding (Naprstek and Smith 2019; Davis 2022) as discussed in Chapter 2. However, inverting grid data away from the measurement lines

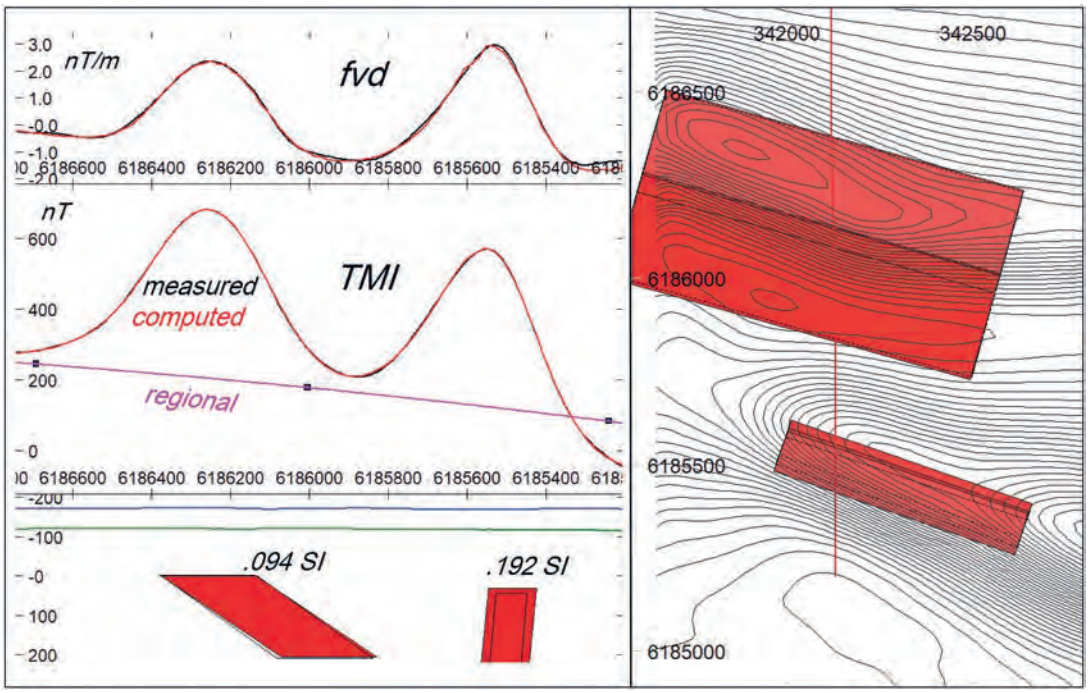

Fig. 3.34. Detailed survey tie-line 10940 inversion models (red) and intersections of models from inversion of the coincident regional survey tie-line.

tests only the fidelity of the gridding algorithm used and not the true magnetic field.

Even without knowledge of the true depths to magnetisation, the Sedan study has established limitations of mapping depth-to-magnetisation from regional 400 m line-spaced surveys over areas where magnetisation is at depths below sensor in the range of 200 m or less (100 m or less below surface). The surveys are able to reasonably determine depths to magnetisation at 50 m below ground for magnetisations that are elongate perpendicular to the flightline direction but are inadequate to determine magnetisation depth from small, equidimensional anomalies or from anomalies elongate oblique to the flightline direction. The detailed survey with closer line spacing and at lower elevation provides for some anomalies more consistent and reliable depth estimates than the regional survey and for other anomalies provides estimates that cannot be made from the regional survey.

3.5 CONCLUSIONS

The challenges and capabilities of magnetic source depth estimation are complex. The highly disruptive consequences of non-uniqueness are not just in not being able to know the correctness or otherwise of a solution but also therefore of not being able to assign a conventional statistical uncertainty to that solution. The capabilities of magnetic source depth estimation vary between projects dependant on the suitability of the geology and the quality and sufficiency of the magnetic field data. To better accumulate lessons of magnetic field source depth estimation requires development of a significant database of depth predictions that are subsequently tested by drilling. No such comprehensive database is presently available in published literature.

In this study I have focussed on the 'greenfields' challenge of estimating depth to an unknown magnetisation without access to independent information. The sweet-spot method I have illustrated can be applied to any reasonably defined discrete magnetic field anomaly, of which a typical aeromagnetic survey may contain tens to many thousands. Parametric inversion used in this study is well suited for any such studies. This chapter has investigated generation of estimates of depth to top of a magnetisation. In addition to this focus on the best expected depth, further studies can be designed to independently estimate the feasibility that the top of magnetisation is at some shallower depth or to estimate the greatest feasible depth.

REFERENCES

Almond R, Fitzgerald DJ (1998) Naudy based automodelling with trend enhancements. *Exploration Geophysics* **29**, 372–377. doi:10.1071/EG998372

Davis A (2022) Nested anisotropic geostatistical gridding of airborne geophysical data. *Geophysics* **87**, E1–E12. doi:10.1190/geo2021-0169.1

Hansen RO (2005) 3D multiple-source Werner deconvolution for magnetic data. *Geophysics* **70**, L45–L51. doi:10.1190/1.2073883

Ku CC, Sharp JA (1983) Werner deconvolution for automated magnetic interpretation and its refinement using Marquardt's inverse modelling. *Geophysics* **48**, 754–774. doi:10.1190/1.1441505

Marquardt DW (1970) Generalized inverses, ridge regression, biased linear estimation, and nonlinear estimation. *Technometrics* **12**, 591–612. doi:10.1080/00401706.1970.10488699

McGrath PH, Hood PJ (1970) The dipping dike case: a computer curve-matching method of magnetic interpretation. *Geophysics* **35**, 831–848. doi:10.1190/1.1440132

Nabighian MN (1972) The analytic signal of two-dimensional magnetic bodies with polygonal cross-section: its properties and use for automated anomaly interpretation. *Geophysics* **37**, 505–517. doi:10.1190/1.1440276

Naprstek T, Smith RS (2019) A new method for interpolating linear features in aeromagnetic data. *Geophysics* **84**, JM15–JM24. doi:10.1190/geo2018-0156.1

Naudy H (1971) Automatic determination of depth on aeromagnetic profiles. *Geophysics* **36**, 717–772. doi:10.1190/1.1440207

Pratt DA, White AS, Parfrey KL, McKenzie KB (2020) 'ModelVision User Guide Version 17.0.' Tensor Research (unpublished).

Reid AB (1980) Aeromagnetic survey design. *Geophysics* **45**, 482–516. doi:10.1190/1.1441102

Reid AB, Allsop JM, Granser H, Millett AJ, Somerton IW (1990) Magnetic interpretation in three dimensions using Euler deconvolution. *Geophysics* **55**, 80–91. doi:10.1190/1.1442774

Silva JBC, Barbosa VCF (2003) 3D Euler deconvolution: theoretical basis for automatically selecting good solutions. *Geophysics* **68**, 1962–1968. doi:10.1190/1.1635050

Thompson DT (1982) EULDPH: a new technique for making computer-assisted depth estimates from magnetic data. *Geophysics* **47**, 31–37. doi:10.1190/1.1441278

Vallée MA, Keating P, Smith RS, St-Hilaire C (2004) Estimating depth and model type using the continuous wavelet transform of magnetic data. *Geophysics* **69**, 191–199. doi:10.1190/1.1649387

Werner S (1953) 'Interpretation of magnetic anomalies at sheet-like bodies.' Sveriges Geologiska Undersok, Ser. C. Arsbok, 43, no. 6. Published by Sveriges geologiska undersöking, Stockholm.